12

Fabrication of nanowires and nanotubes by anodic alumina template-assisted electrodeposition

Wojciech J. Stępniowski[1] and Marco Salerno[2]

[1]Department of Advanced Materials and Technologies, Faculty of Advanced Technologies and Chemistry, Military University of Technology, 2 Kaliskiego Street, 00-908 Warszawa, Poland
[2]Department of Nanophysics, Istituto Italiano di Tecnologia, via Morego 30, I 16163 Genova, Italy

Outline:

Introduction

Quasi-one dimensional nanostructures such as nanowires and nanotubes have attracted the attention from researchers due to their properties of the two dimensions being in the nanoscale and one dimension being in the microscale. Fabrication of ordered arrays of nanostructures is required in catalysis, sensing, electronics, energy harvesting and storage, and applications of materials with tailored magnetic and optical properties.

Typically manufacturing techniques applied require expensive equipment and time consuming processes. A promising alternative is the fabrication of nanostructures using anodic alumina templates. In this case, templates that are relatively easy to make in house with fully controlled geometrical features serve as 3D masks in various deposition procedures. A common technique such as electrochemical deposition can be applied to form nanowires and nanotubes, while anodic alumina membranes are used as the mould during the electrodeposition. An easy-to-read compendium of these cost-effective methods is highly desirable, which requires a systematic review with detailed data about fabrication and applications. In this chapter a detailed review of the fabrication techniques based on anodic alumina templates, as well as the respective electrodeposition conditions - including composition of deposition bath, type of applied current and additional critical experimental data - is provided. All the relevant experimental data with the respective literature references have been arranged in tables.

Fabrication of anodic aluminum oxide (AAO)

Electrochemical oxidation of aluminum – anodization – in electrolytes at pH lower than 5 allows to form hexagonally honey-comb arrays of pores, ideally aligned normal to the surface, forming parallel capyllars [1]. To obtain this structure, aluminum has to be subjected to anodization under controlled experimental conditions. An ideal honey-comb array of anodic aluminum oxide (AAO) is shown in Fig. 12.1. One can distinguish pores that are organized in a close-packed hexagonal lattice. A typical AAO lattice is characterized by such major geometrical factors like pore diameter (D_p), interpore distance (pore center to pore center distance), equal to the diameter of the circle enclosing the hexagonal cell with the pore in its center (D_c), thickness of the grown oxide (H), thickness of the barrier layer at the pores bottoms (B), and number of pores occupying a unit area, also known as pore density (n). Most of the geometric features are in mutual correlations. For example the thickness of the AAO cell wall (W) is linked with both pore diameter and interpore distance via the following equation [1]:

$$W = \frac{D_c - D_p}{2} \qquad (1)$$

Experimentaly it has been observed that the barrier layer B is thicker than the cell wall W, and is connected to it (and thus to both D_c and D_p) by a simple dependency [1]:

$$B = \frac{W}{0.71} = \frac{D_c - D_p}{1.42} \qquad (2)$$

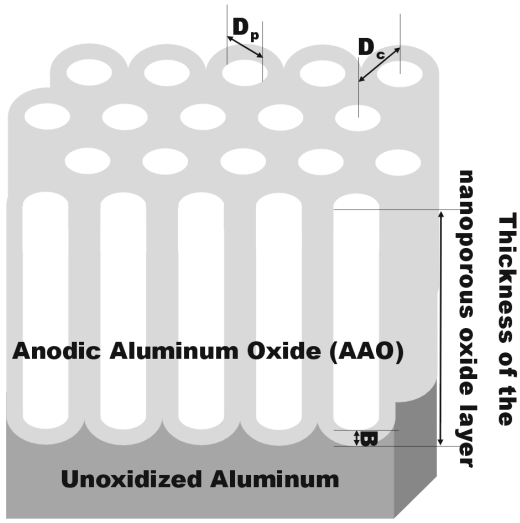

FIGURE 12.1
Ideal structure of AAO where major geometrical parameters are shown: pore diameter (D_p), interpore distance (D_c), thickness of the nanoporous oxide (H) and thickness of the barrier layer (B)

For ideally perfect, close-packed hexagonal AAO lattice, porosity (P) can be also evaluated from the pore diameter and interpore distance [1-2]:

$$P = \frac{\pi}{2\sqrt{3}} \cdot \left(\frac{D_p}{D_c}\right)^2 = 0.91 \cdot \left(\frac{D_p}{D_c}\right)^2 \qquad (3)$$

To form regular AAO successfully, all the aluminum surface has to be smooth, to avoid major curvatures of electric field lines that would generate locally enhanced corrosion. Typically, aluminum is electropolished in a mixture of perchloric acid and ethanol 1:4 by volume [1-2]. Two different approaches may be adopted, namely galvanostatic (for relatively small surfaces) and potentiostatic (for relatively large surfaces). A typical galvanostatic electropolishing applied for relatively small samples was reported for example by Sulka and Stępniowski [2]: 0.5 A/cm^2 at 10^{o}C for 1 minute. For relatively large surface, up to 4 cm^2, Zaraska et al. applied instead potentiostatic electropolishing: 20 V, 10 ^{o}C, for 1 min [3].

According to Parkhutik and Shershulsky [4] the growth of AAO consists of few distinct parts (Fig. 12.2). Firstly, on the electropolished aluminum a barrier oxide is formed (stage 1), accompanied by a rapid current density decrease and simultaneous voltage increase. Next, the barrier oxide begins to crack (stage 2), decreasing the drop rate of the current density, as well an increased rate of the voltage. In stage 3, during nucleation of pores the current density rises and the voltage drops to the respective values at which the steady state growth of the nanopores is achieved (stage 4). Different from this picture, according to the recent theory of Pashchanka and Schneider, hexagonal nanopore arrays of anodic alumina are an effect of a non-linear phenomenon analogous to the formation of Rayleigh-Bénard convective cells in viscous fluids in the presence of a temperature gradient counteracting the gravity. The applied voltage plays a major role and is linked with charge transfer properties of the solution such as conductivity. The current-time curves of Fig. 12.2 can be ascribed to

the early formation of the barrier layer, as displacement and mutual interaction of adsorbed and incoming anions. In this picture, the barrier layer is only formed at high pH in the end of the anodization. Ion concentration and current fluctuations cause a competition between the two driving forces, namely Coulomb attraction of the anions by the anode and diffusion of the ions towards electrolytes bulk, finally reaching a steady state in stage 4 [5], when growth of anodic alumina is achieved. Ion migration caused by diffusion and Coulomb force causes a pH gradient: in the electrolyte bulk the pH is below 4, however attracted anions, including OH^- species, cause a local pH increase at the anode. At pH of between 5 and 9 formation of AlO(OH) and Al_2O_3 occurs [5].
During anodic oxide growth all the anions in the electrolyte are attracted to the positive anode, and thus can be adsorbed and incorporated into the anodic oxide to different extent. Diggle et al. [6] and Parkhutik et al. [7-8] showed that the amount of adsorbed atomic species from the electrolytes anions is significant, typically in the range of 4-8%. These contaminating anions can bring functionality to the anodic alumina, for example in the form of photoluminescence [9-10]. It has been demonstrated that the external addition of stable chelate anions to the electrolyte leads to their incorporation and corresponding modification of the grown oxide properties [11].
There are two strategies to form highly ordered AAO. A virtually defect-free, highly-ordered oxide layer can be formed when starting from pre-patterned aluminum, but the area of the ordered surface is strictly limited. Large sheets of aluminum can also be anodized without pre-patterning, exploiting mainly the self-organization of the oxide during its growth.

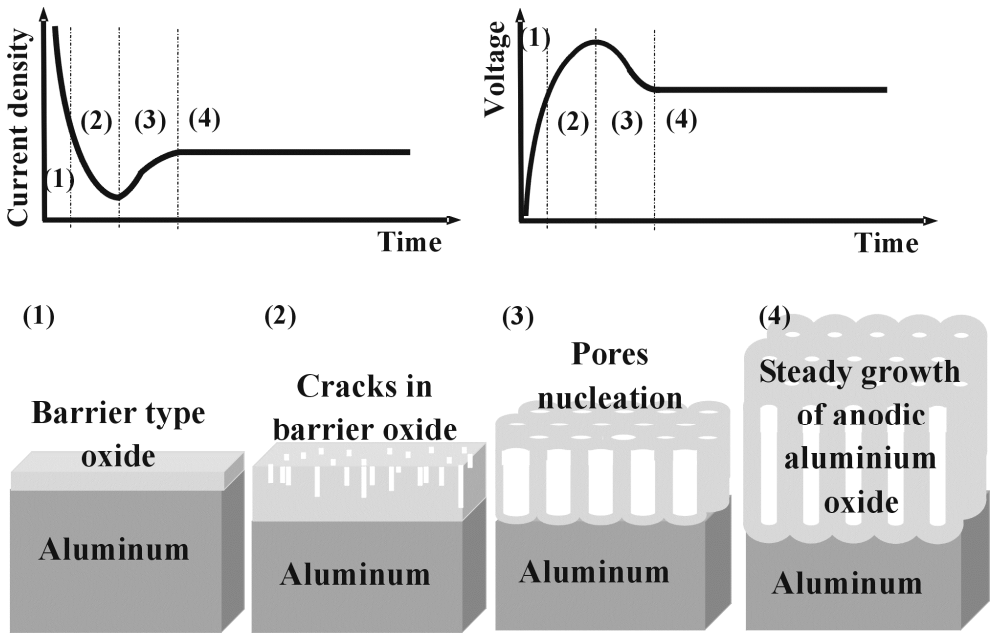

FIGURE 12.2
Current density vs. time and voltage vs. time for the growing AAO

The first approach is based on the fabrication of surface pits in the aluminum at the position of future AAO pores, which can be made by direct indentation with a tip of atomic force or other scanning probe microscope [12-13], or by milling with focused ion beam [14-16]. Alternatively, molds of hard materials like Si_3N_4 [15–17], SiC [18–23], or Ni [24–25], usually made with electron beam lithography, can be used

for imprinting of the aluminum. Application of pre-patterning enables fabrication of ordered circular pores with hexagonal or square arrangement, as well as square and triangular pores. After the pre-patterning the aluminum with formed concaves is anodized and ideally ordered nanoporous AAO is formed. However, all the pre-patterning methods require expensive facilities and the treated area is limited to a few mm^2, which makes them very time and cost ineffective. This is also the case for the pre-patterning based on molds, even if the advantage of using imprinting molds for pattern transfer is that the same mold can be used for several times.

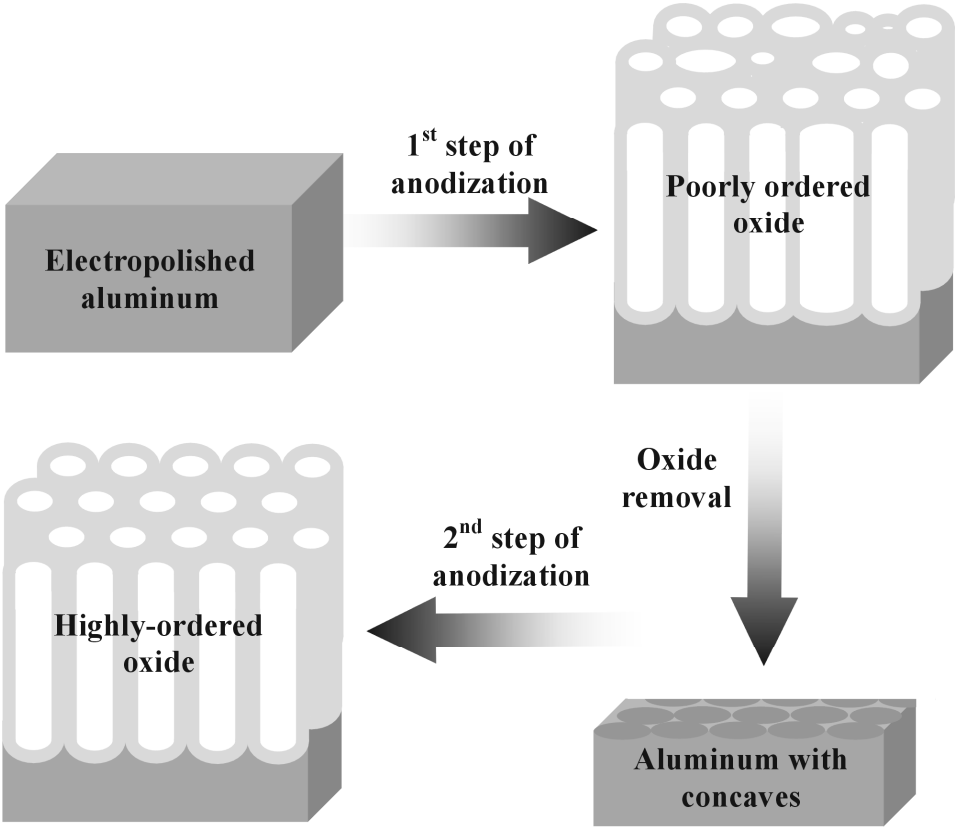

FIGURE 12.3
Schematic of self-organized pre-patterning of aluminum for the formation of highly ordered AAO

To overcome the above limitations a method developed in 1995 by Masuda and Fukuda [26], based on self-organization, can be used. Its application has triggered numerous research in the field of AAO. According to the self-organized procedure, an electropolished aluminum sample is anodized at certain experimental conditions, including type, concentration and temperature of electrolyte, applied voltage and time (Fig. 12.3). The oxide formed is initially poorly ordered, i.e. the pores are not ideally cylindrical and their diameter and interpore distance distributions are broad. However, the first anodization itself is used as the pre-patterning step, since during this phase improved pore ordering is progressively obtained, by extending the anodization to longer and longer times [27]. Note that the best ordering occures at the pore bottoms, i.e. the AAO layer grown last, whereas the AAO top surface is the original, disordered one of the initial growth. At this point the whole AAO layer is removed, by

chemical etching usually performed in a mixture of phosphoric and chromic acid [1-3, 26-27]. As a result, aluminum with concaves is obtained, with degree of order and uniformity proportional to the first anodization time, at least in the range of 5-10 h. These concaves serve as the pore nucleation sites during the second step of anodization, which is conducted at the same experimental conditions as the first step, but starts from already ordered (electrochemically pre-patterned) aluminum. Therefore, after the second anodization step a highly ordered array of nanoporous AAO is formed. In Fig. 12.4 one can distinguish highly-ordered domains with defective domain boundaries. For various operating conditions the nanopores have different pore diameter, interpore distance, porosity and pores density (Fig. 12.4 compare a to b).

Fundamental research was carried on the influence of operating conditions on the geometry of AAO. Typically, to form highly-ordered nanoporous AAO templates one of three electrolytes is applied among sulfuric, oxalic and phosphoric acid. The used electrolyte determines the range of applied voltage suitable for fabrication of ordered arrays. For example, to form ordered AAO in sulfuric acid the applied voltage ranges from 15 to 25 V [28-29]. Typically, to form ordered nanopores in oxalic acid the voltage range is from 30 to 80 V [2, 30-31], however application of high velocity stirring enables anodization in oxalic acid even at 5 V [32]. Finally, the voltage range suitable for aluminum anodization in phosphoric acid is from 110 V [33] to 195 V [34]. Above these voltages anodic dissolution of aluminum is the dominating process instead of anodization (passivation). According to Nielsch et al [34], for every applied electrolyte there is a voltage at which the best arrangement is achieved. This corresponds to a resulting porosity close to the value of 10%, which would guarantee the best conditions for growth under appropriate stress (not too high, not too low), when considering the Pilling-Bedworth ratio typical of bulk aluminium, which is 1.2-1.3 [35]. Consistent with this assumption, and after experimental observations, the best AAO pores arrangement is obtained for sulfuric acid at 25 V, for oxalic acid at 40 V, and for phosphoric acid at 195 V.

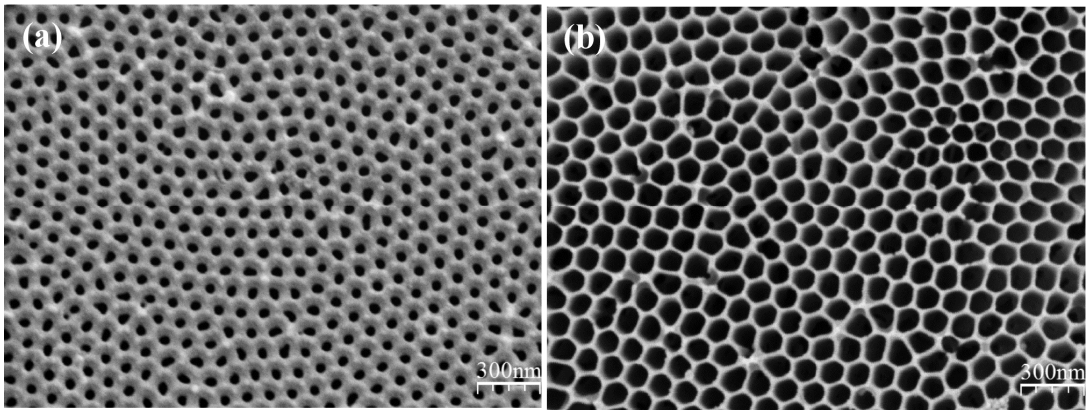

FIGURE 12.4
Top-view FE-SEM images of AAO formed in 0.3 M oxalic acid at 50°C, 40 V via 15 minutes long anodization (a), and at 45°C, 45 V via 2 hours long anodization

The applied voltage, the electrolytes temperature and the duration of the second anodization step, determine the pore diameter D_p (Fig. 12.5a) and interpore distance D_c (Fig. 12.5b). Research has shown that both Dp and Dc increase linearly with the voltage (Fig. 12.5) [2, 28-34, 36-43]. It has been also proven that temperature increase and lengthening of the second anodization step increase the pore diameter D_p, due to enhanced chemical etching reaction between the grown AAO and the electrolyte

(Fig. 12.5a) [2, 36]. On the other hand, there is neither temperature nor time effect on the interpore distance D_c, and in all cases the interpore distance increases linearly with the voltage U (Fig. 12.5b):

$$D_c \approx 2.5 \cdot U \qquad (4)$$

Anodization is a typical faradic process [1], so the longer is the second step of anodization, the thicker will be the porous oxide layer. Current density and porous oxide layer thickness also increase exponentially with the voltage [2]. Additionally, temperature increase enhances the ionic mobility, which results in a current density increase, and as a consequence the oxide is also grown thicker [2]. All these interplaying parameters are sometimes not easily split in interpretation of the resulting effects [1].

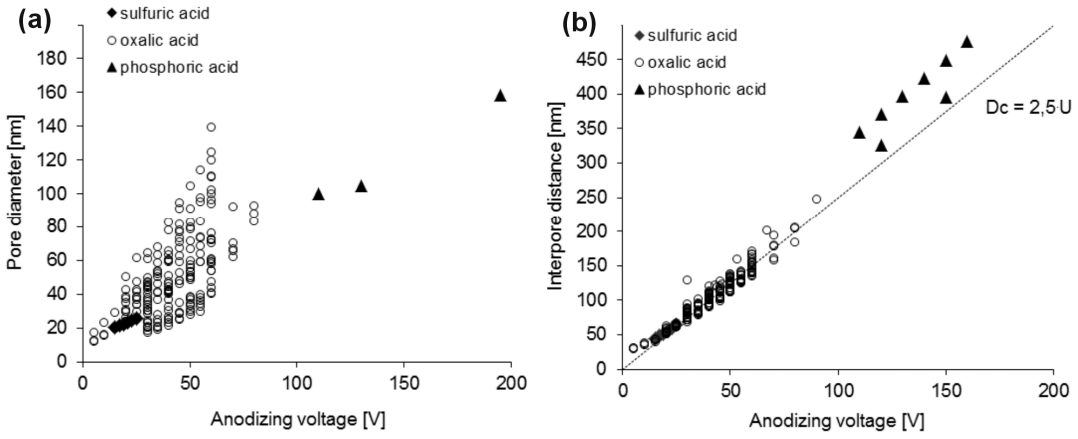

FIGURE 12.5
Influence of voltage on pore diameter D_p (a) and interpore distance D_c (b). Results were gathered from Ref.s [2, 28-34, 36-42]

An extreme regime of AAO growth rate is obtained by application of hard anodization (HA), which means anodization performed at too high voltages for the given electrolyte, which give rise to local burning effect. To avoid anodic dissolution as a typical side-effect of HA, before the HA, usually a different anodization regime is carried out, called mild anodization (MA). MA forms a protective oxide layer, preventing the anode from electrochemical dissolution at the harsh HA conditions. According to Lee et al., HA performed for example in sulfuric acid at 40 to 70 V results in interpore distance ranging from 90 to 140 nm [44]. However the major benefit of HA is the significant increase in oxide growth rate. For example AAO grows in oxalic acid during MA at about 2 μm/h (40 V, 1°C), and in the same electrolyte during HA the oxide growth rate increases to about 70 μm/h (110-150 V, 1°C). Additionally, by different combinations of HA and MA regimes, template with various pore shapes can be obtained. For example, multi-segment nanowires were obtained by using alternatively MA and HA during the same process [45]. Similarly, with the combined use of MA and HA (in the absence of HA-MA cycles), also Y-branched nanopores could be formed [46]. According to Zaraska et al., Y-branched nanopores can be also formed using voltage decrease in the MA voltage range alone [47]. Due to the geometrical dependencies, decreasing the voltage by a factor √2 from 60 to 42 V and next from 42 to 30 V, multi-Y-branched fractal-like nanopores were formed.

As mentioned above, sulphuric, oxalic and phosphoric acid are the most frequently applied electrolytes for aluminum anodization, due to the nanopores ordering that they provide - particularly for oxalic acid - and to their common availability arising from huge industrial production for different applications. However, other research works have focused on anodization of aluminum in various other acids, such as chromic [7-8, 48] and selenic acid [49], as well as many organic acids: squaric [50], malic [43, 51] citric [52], malonic [43, 52], maleic [43], tartaric [43, 52], tartronic [43], glutaric [51], lactic [52], propionic [52], glycolic [52] and succinic [51-52]. Whereas not all these acids demonstrated to result in nanoporous AAO, still the choice of the acid type is one of the several experimental parameters of aluminum anodization resulting in a large number of combinations of experimental conditions, which makes AAO a suitable material for template nanofabrication.

Fabrication of passing-through AAO layers and membranes

Application of AAO as the template for nanofabrication is possible only if post-anodization treatment of the formed material is applied. In electrochemical deposition anodic alumina serves as an insulating mask for the working electrode, thus the nanopores have to be opened. Formation of through-hole AAO layers can be performed with two most commonly applied approaches: chemical aluminum removal plus chemical pore opening, or electrochemical thinning of the barrier layer (Fig. 12.6). When the former route is followed, first an AAO membrane suitable for further electrochemical nanofabrication is obtained. To this goal, the remaining unoxidized aluminum has to be removed first. This step is commonly fulfilled by a typical redox reaction with $HgCl_2$ (eq. 5) [53-59], $CuCl_2$ [60-65] or $CuSO_4$ [66] (eq. 6), $SnCl_4$ (eq. 7) [67-69] or even in methanol solution of Br_2 (eq. 8) [70]:

$$3Hg^{2+} + 2Al \rightarrow 2Al^{3+} + 3Hg \quad (5)$$

$$3Cu^{2+} + 2Al \rightarrow 2Al^{3+} + 3Cu \quad (6)$$

$$3Sn^{2+} + 4Al \rightarrow 4Al^{3+} + 3Sn \quad (7)$$

$$3Br_2 + 2Al \rightarrow 2Al^{3+} + 6Br^{-} \quad (8)$$

Typically, aluminum removal is carried out in aqueous chloride based saturated solution. In particular, to provide better electron exchange, most often etching is conducted in $CuCl_2$with addition of HCl. After aluminum removal the pores have to be opened (Fig. 12.6) in 5%vol phosphoric acid. This step requires careful optimization. According to one option, the whole AAO membrane is submerged in H_3PO_4, but in this case the pore opening is accompanied by pore widening, as the solution penetrates the pores from the top and the acid reacts with the grown oxide [53]. According to another option, the AAO membrane is gently laid on top of the etching solution and let it float there thanks to the surface tension that prevents the sample from sinking in [71]. In this case only the pore bottoms are reacting with the acid, but this method is not easily reproducible. Then, the prepared through-hole membrane can be used as a template in further nanofabrication.

Nanofabrication with the use of methods other than the electrochemical ones employs the above AAO membranes. However, for electrochemical deposition the presence of an electrode - i.e. an electrically

conductive material - at one sideface of the membrane has to be provided. In some cases a golden layer is sputtered on the pore bottom, and then electrodeposition of a thin gold layer is carried out inside the pores. This results in formation of short nanopillars partly penetrating the pores, thus forming very good electrical contacts for the subsequent electrodeposition of the demanded element, which makes it possible to obtain a high filling of the pores [58]. According to this method, prior to the electrodeposition of desired material a four-step-long procedure has to be employed to make the AAO membrane suitable.

An elegant and much shorter alternative, employing only in situ electrochemistry treatment prior to desired metal electrodeposition, is the barrier layer thinning (BLT). This approach, reported first by Furneaux et al. [72], is based on the gradual voltage decrease right after the second anodization step (Fig. 12.6). After each voltage decrease the equilibrium current flow (stage 4 in Fig. 12.2) is perturbed (at lower voltage the current density drops), and the system tries to get back to the equilibrium with nucleation of new pores, what is seen as a current density increase. The trick is to not allow a new equilibrium - i.e. steady state of the porous oxide growth - to be established, and decrease the voltage again. These steps have to be repeated until a very low voltage is achieved, about 1 V [72-74]. As the resulting effect, fractal-like cracks in the barrier layer are formed, due to newly nucleated pores. These short pores are already in contact with the aluminum layer, which can work as an electrode for further nanofabrication.

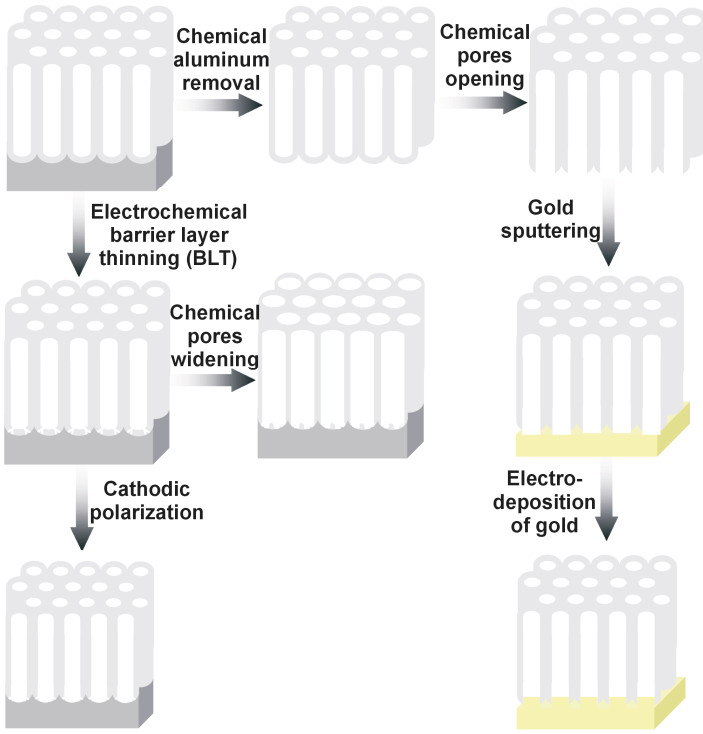

FIGURE 12.6
Various approaches in preparation of passing-through AAO template on metallic electrode for subsequent fabrication of nanowires and nanotubes

The voltage drop step is critical, and typically is 5% of the previous voltage value, down to a minimum value of 0.3 V [72]. The voltage can also be decreased exponentially by a programmed power supply [73-74], and similar effects are obtained. The process can also be eased by using only a few steps involving a voltage decrease [75]. According to Montero-Moreno et al. the current density can be decreased at each step by half its previous value, and concurrently the step duration has to be doubled, except for the last step. The whole BLT process consisted in their case of only five steps, what significantly eases the process and makes it more time efficient [75]. To improve the pore filling with the deposit, various post-anodization treatments can be done. To widen the contacts on the aluminum support, the AAO after BLT can be immersed in phosphoric acid [76-78]. Another more sophisticated technique was also developed, i.e. cathodic polarization of the AAO after BLT in 0.5 M KCl (Fig. 12.6). During the process, while the AAO sample serves as a cathode and is subjected to cathodic polarization in potassium chloride solution, OH^- anions attack both the barrier layer and the pore walls, thinning them significantly [79-81]. Moreover, chlorides also play role in barrier layer dissolution during cathodic polarization, due to their adsorption on the alumina and formation of water soluble $Al(OH)_2Cl$ [79].
In conclusion, with the application of typical chemical or electrochemical methods, hexagonally ordered alumina templates suitable for subsequent electrochemical nanofabrication can be formed efficiently.

Template-assisted electrochemical fabrication of metallic nanowires

Electrochemical deposition into the nanoporous AAO templates allows the manufacture of high aspect ratio nanowires in a variety of metals. Nanowires made of Al [82], Ag [53-55, 60-61, 82-85], Ag-Au [61, 86], Ag-Ni [87], Au [53, 56-57, 61, 88-90], Bi [91], Co [76, 92-98], Co-Cu [93, 99], Co-Fe [100], Co-Ni [62, 101], Co-Ni-Fe [102], Co-Pt [92, 103], Co-Zn [104], Cu [58, 67, 105-108], Fe [63, 76, 109], Fe-Pd [110], Fe-Pt [103], Ni [59, 61, 65, 68-70, 76, 91, 93, 111-121], Ni-Fe [64], Ni-Pt [103], Pd [66, 122-123], Pt [92, 124-125], Sn [53, 55, 126], and Zn [127] were successfully formed (Table 12.1 and Fig. 12.7).

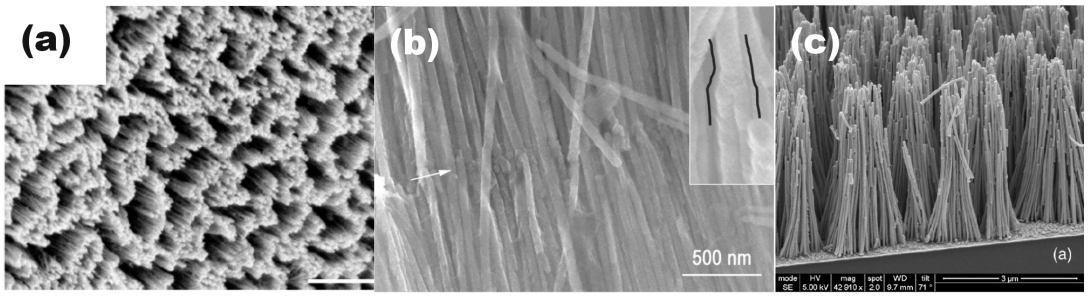

FIGURE 12.7
FE-SEM micrographs of Ag (a) [84], Y-branched Ni (b) [69] and Pt (c) [124] nanowires. Copied with permissions from Elsevier

A typical nanowire manufacturing process consists of two steps: electrochemical reduction of the cation at the pore bottoms, and template removal (Fig. 12.8). Typically, for AAO removal phosphoric acid is used, however for this application NaOH is usually employed. In fact, use of phosphoric acid would enable secondary reaction between the acid and nanowires. These would be covered by various

oxidation products affecting significantly their properties and size. To form metallic nanowires both direct, alternate and pulsed current have been used for the electrochemical deposition. Often, commercially available solutions are used to deposit the desired metal [53, 55, 61, 83, 89, 122]. With the use of AAO templates nanowires with various morphologies were obtained, including diameter modulated nanowires made of Ag, Ag-Au, Au and Ni [61], Y-branched nanowires made of Au [57], Cu [67] and Ni [69, 117] and core-shell nanowires made of Ag-Ni [87].

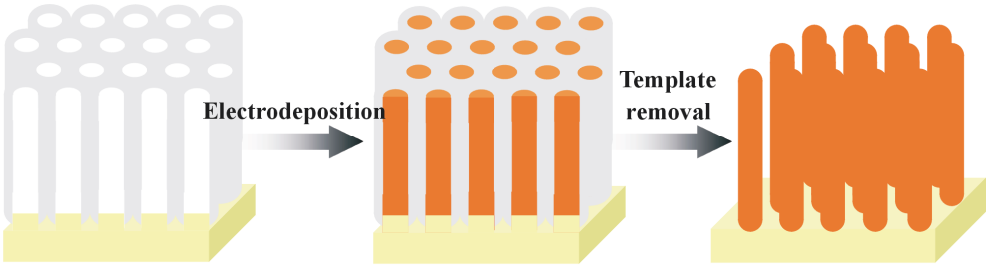

FIGURE 12.8
Schematic representation of the nanowires deposition into the AAO nanoporous template

Due to the large surface area of the metal nanowire arrays, the resulting nanostructures were employed as an electrode material for various purposes. For example, aluminum nanowires were coated by TiO_2 by means of atomic layer deposition, and used as an electrode in lithium-ion batteries [82]. With this material greater current density and power can be obtained and the number of charge-discharge cycles can be significantly increased. Nanowire arrays made of Pt were also used to decompose methanol electro-catalytically [124], showing in turn higher performance than for traditional materials. Metal nanowires are particularly attractive for applications in magnetism, optics, or as a field emission material. Detailed fabrication and magnetic characterization of nanowires made of A Ni [87], Co [76, 93-96, 98], Co Cu [2, 99], Co Fe [100], Co Ni [62, 101], Co Ni Fe [102], Co Zn [104], Fe [63, 76], Fe Pd [110] and Ni [59, 68, 70, 76, 93, 112, 118-121] were successfully performed. Moreover, Ni nanowires are also attractive due to their optical [121] and field emission properties [116].

A wide range of nanowires manufactured with electrochemical techniques were formed with the AAO template-assisted procedure. The major advantage of the above methods is the relatively high filling ratio of the pores, the uniformity of the obtained nanowires, and the repeatability of the results. Cost effectiveness employing electrochemistry and self-organization, makes the methods even more attractive for high tech industries.

TABLE 12.1
Gathers metallic nanowires with their fabrication conditions. Type of AAO: L – lab made (LS – sulfuric acid, LO – oxalic acid, LP – phosphoric acid), C – commercial. Type of membrane preparation: RO – chemical Al removal + pore opening (specified chemicals), O – chemical pore opening, BLT – electrochemical barrier layer thinning (specified conditions). Type of applied current: DC - DC electrodeposition, AC – AC electrodeposition, CV – Cyclic Voltammetry, Pulse – Pulse electrodeposition; RT – room temperature. ***(Part 1 of 10, to be continued)***

NW metal	Type of AAO	Membrane preparation	Type of applied current	Deposition bath	Deposition conditions	Remarks / Investigated properties	Reference
Al	C	C: Anodisc 47, Whatman	Pulse: -0.4 V for 50 ms / -0.1 V for 200 ms	$AlCl_3$ + 1-ethyl-3-methylimidazolium chloride (ionic liquid)	-	TiO_2 was deposited with Atomic Layer Deposition (ALD) on the Al NW, to form highly-efficient 3D electrode material for batteries	[82]
Ag	LP	BLT (H_3PO_4 from 195 down to 80 V, $(COOH)_2$ from 80 to 1 V). Voltage step from 2 down to 0.1 V. 180 s long steps in H_3PO_4 and 30 s long steps in $(COOH)_2$	DC: 10 mA/cm^2	Commercial electrodeposition bath (Silver 1025, Technic Corp.)	25 ^oC	Obtained NW length ≥ 30 μm, diameter 180-400 nm	[83]
Ag	LP	RO: $CuCl_2$ in HCl + H_3PO_4	CV: 0.0 to –0.6 V	0,01 M $AgNO_3$	RT	Obtained NW aspect ratio 5-500	[60]
Ag	LO	O: H_3PO_4	AC	2 g/L $AgNO_3$, 20 g/L H_3BO_3	pH = 2.5 (H_2SO_4)	Various procedures of pore opening and electrodeposition were investigated	[84]
Ag	LO	RO: $HgCl_2$ + H_3PO_4	DC: 1 mA/cm^2	Commercial electrodeposition bath (Alfa Aesar, Ag content 28.7 g dm^{-3})	10 min, RT	AAO templates were formed on technical purity Al, instead of high purity Al, what allowed to cut costs significantly	[53]
Ag	LO	RO: $HgCl_2$ + H_3PO_4	DC: 2.5 mA/cm^2	300 g/l $AgNO_3$, 45 g/l H_3BO_3	pH = 2.5, RT, 8 h	Ordered Ag NW arrays were obtained	[54]
Ag	LS	-	AC: 20 V, 200 Hz	4 g/l AgNO3, 20 g/l MgSO4,	pH = 2.5 – 3.0, 20 ^oC, 15 min	Antibacterial properties of Ag NW were researched	[85]
Ag	LO	RO: $HgCl_2$ + H_3PO_4	DC: 4 mA/cm^2	Commercial electrodeposition bath (Alfa Aesar, Ag content 28.7 g dm^{-3})	30 min	AAO templates were formed at 20 ^oC and filled with Ag NW	[55]

Table 12.1, *(continued, part 2 of 10)*.

NW metal	Type of AAO	Membrane preparation	Type of applied current	Deposition bath	Deposition conditions	Remarks / Investigated properties	Reference
Ag	LS	RO: 0.1M $CuCl_2 \cdot 2H_2O$ in 6.1M HCl + 0.52 M H_3PO_4	DC: 1mA/cm^2	Commercial electrodeposition bath (Alfa Aesar, Ag content 28.7g dm^{-3})	20 min	Diameter modulated Ag NW were formed	[61]
Ag-Au	LS	-	AC: 7.0 V, 40 Hz	Au: 1.0 mM $HAuBr_4$ Ag: 1.0 mM Ag_2SO_4	Ag: pH = 2.5, 293 K, 5 min Au: pH = 2.0, 293 K, 5 min	UV-Vis absorption spectra of Ag-Au NW were investigated	[86]
Ag-Au	LS	RO: 0.1M $CuCl_2 \cdot 2H_2O$ in 6.1M HCl + 0.52 M H_3PO_4	DC: 3–4 mA/cm^2	20 mmol dm^{-3} KAg(CN)2 +10 mmol dm^{-3} KAu(CN)2	30 min	Diameter modulated Ag-Au NW were formed; due to the dealloying, porous Au NW were formed	[61]
Ag-Ni	C	C: Whatman	Ag, DC: 4mA / cm^2 Ni, DC: 1.6 V–2.6 V	Ag: $Ag(NO_3)_2$ (0.005–0.02M), $Ac(NH_3)$ (0.4 M) Ni: $NiSO_4 \cdot H_2O$ (0.8 M), $NiCl_2 \cdot H_2O$ (0.48 M), H_3BO_3 (0.6 M) and H_2O_2 (30%, 0.01 M)	Ag: RT Ni: 60 °C, pH: 2.0 – 5.2	Magnetic properties of core-shell nanowires were researched	[87]
Au	LO	RO: $HgCl_2$ + H_3PO_4	DC: 0.5 mA/cm^2	Commercial electrodeposition bath (Umicore, Auruna ® 5000, Au content 7g dm^{-3})	20 min, RT	AAO templates were formed on technical purity Al, instead of high purity Al, what allowed to cut costs significantly	[53]
Au	LS	RO: 0.1M $CuCl_2 \cdot 2H_2O$ in 6.1M HCl + 0.52 M H_3PO_4	DC: 5–7 mA/cm^2	Commercial electrodeposition bath (Umicore, Auruna ® 5000, Au content 7g dm^{-3})	30 min	Diameter modulated Au NW were formed	[61]
Au	LO	BLT: the anodic voltage was gradually lowered to 20 V by 2 V/min and then to 1 V by 1 V/min.	AC: 8 V, 200 Hz, 30 s Then: DC: 2–16 mA cm^{-2}.	1 g/L $HAuCl_4 \cdot 4H_2O$, 30 g/L boric acid	pH = 1.5, RT	Arrays of Au NW were formed in AAO templates formed by BLT. Prior DC electrodeposition, AC electrodeposition was performed to fill the opened bottoms of AAO	[88]

Table 12.1, *(continued, part 3 of 10).*

NW metal	Type of AAO	Membrane preparation	Type of applied current	Deposition bath	Deposition conditions	Remarks / Investigated properties	Reference
Au	LO	O: H_3PO_4	DC: 6 mA/cm^2	Commercial electrodeposition bath (Pur-A-Gold) with K[Au(CN)$_2$]	pH = 5.75, 60 ^{o}C, 60-80 s.	The Au NW arrays were used as the high surface area electrodes	[89]
Au	LO	RO: $HgCl_2$ + H_3PO_4	DC: 10 μA/cm^2	12 g/L $HAuCl_4$, 160 g/L Na_2SO_3, 5 g/L ethylene-diaminetetraacetic acid, 30 g/L K_2HPO_4, 0.5 g/L $CoSO_4$	pH = 9.0	The Au NW were used as enzyme electrode in electrochemical glucose bio-sensors	[56]
Au	LO	RO: $HgCl_2$ + H_3PO_4	DC: 1mA/cm^2	Commercial electrodeposition bath (Umicore, Auruna ® 5000, Au content 7 g dm^{-3})	20 min	Y-branched Au NW were obtained	[57]
Au	LS	O: H_3PO_4	AC: 11 V	1 g/L $HAuCl_4$, 7 g/L H_2SO_4	20 min	DNA was arranged on the Au NW top surface	[90]
Bi	LS	BLT: 8, 15, 20 V	AC: 6-8 V 10-100 Hz DC: 2-3 V	0.05 M $BiCl_3$ in DMSO	130 ± 0.5 °C	Bi NWs were deposited via electrochemical deposition from non-aqueous bath	[91]
Co	C	C: Whatman	DC	1 M $CoSO_4$	pH = 3.0 (H_2SO_4), RT, 360 min	Various experimental procedures were tested	[92]
Co	LO	O: H_3PO_4	DC: -1.0 V	$CoSO_4 \cdot 7H_2O$ (120 g/l), H_3BO_3 (45 g/l)	-	Magnetic properties of obtained NW were studied	[93]
Co	LO	BLT: acetone: $HClO_4$ 1:1 (vol.) 110 V, 4 ^{o}C, 5 min, subsequent etching in 5% H_3PO_4	DC: 2.5 V	140 g/L $CoSO_4$ 50 g/L H_3BO_3	pH = 4.0, 25 ^{o}C, 1.5 h	Magnetic Properties of NWs were studied	[76]
Co	C	C: Whatman	DC: -1.05 V	400 g/L $CoSO_4$ 40 g/L H_3BO_3	-	Magnetic properties of Co NWs were studied	[94]
Co	C	C: Nanomaterials S.r.l.	DC: -1.1 V	1 M Co(NH_2SO_3)$_2$	pH 6.2, 30 ^{o}C	Magnetic properties of Co NWs were studied	[95]
Co	LS	-	AC: 14 V, 50 Hz	50 g/L $CoSO_4 \cdot 7H_2O$ 20 g/L H_3BO_3	10 min, 35 ^{o}C	Magnetic properties of Co NWs were studied	[96]

Table 12.1, *(continued, part 4 of 10).*

NW metal	Type of AAO	Membrane preparation	Type of applied current	Deposition bath	Deposition conditions	Remarks / Investigated properties	Reference
Co	LO	-	Pulse: 2.5 mA/cm^2, t_{on}:t_{off} = 1:3	0.5 M $CoSO_4$ $5.6 \cdot 10^{-3}$ M ascorbic acid 0.3 M H_3BO_3	-	Co NW were formed in AAO / Liquid Crystal templates	[97]
Co	LO	RO: -	DC: -1.0 V	250 g/l $CoSO_4$ 40 g/l H_3BO_3	RT	Magnetic properties of Co NWs were studied and compared to the theoretical calculations	[98]
Co-Cu	LO	O: H_3PO_4	AC: -0.3 to –1.0 V	$CoSO_4 \cdot 7H2O$ (120 g/l), $CuSO_4 \cdot 5H_2O$ (1.6 g/l), H_3BO_3 (45 g/l).	-	Magnetic properties of obtained NW were studied	[93]
Co-Cu	-	-	Pulse: 40 and 0.5 mA/cm^2	1M $CoSO_4 \cdot 7H_2O$ $CuSO_4 \cdot 5H_2O$ in a ratio of 40:1	pH = 3.0	Magnetic properties of obtained NW were studied	[99]
Co-Fe	-	-	AC	-	-	Magnetic properties of obtained NW were studied	[100]
Co-Ni	LO (HA)	RO: $CuCl_2$ in HCl, H_3PO_4	Various electrodeposition baths and procedures were tested. Magnetic properties of the NW were studied.				[62]
Co-Ni	LS	O: H_3PO_4	Pulse	$Co_{50}Ni_{50}$: 30 g/L $CoSO_4.7H_2O$, 300 g/L $NiSO_4 \cdot 7H_2O$, 50 g/L $NiCl_2 \cdot 7H_2O$, 30 g/L H_3BO_3 $Co_{75}Ni_{25}$: 150 g/L $CoSO_4.7H_2O$, 150 g/L $NiSO_4 \cdot 7H_2O$, 22.5 g/L $CoCl_2 \cdot 7H_2O$, 22.5 g/L $NiCl_2 \cdot 7H_2O$, 45 g/L H_3BO_3	pH = 4.0 65 ^oC	Magnetic properties of obtained NW were studied	[101]
Co-Ni-Fe	C	C: Whatman	DC: 2.0 V	10 mM $Co(SO_4)_2.6H_2O$, 0.2 M $Ni(SO_4)_2 \cdot 6H2O$, 5 mM $Fe(SO_4)_2 \cdot 6H_2O$ 0.2 M H_3BO_3, 35 mM NaCl 0.1 g/l sodium	pH = 2.6 25 ^oC 180-300 min	Magnetic properties of obtained NW were studied	[102]

Table 12.1, *(continued, part 5 of 10).*

NW metal	Type of AAO	Membrane preparation	Type of applied current	Deposition bath	Deposition conditions	Remarks / Investigated properties	Reference
Co-Pt	C	C: Whatman	DC: 5 mA/cm^2	0.1 M cobalt sulphamate, 0.01 M $(Pt(NH_3)_2(NO_2)_2)$, 0.1 M ammonium citrate, 0.1 M glycine	pH = 8 (NaOH), RT, 5h,	Various experimental procedures were tested	[92]
Co-Pt	LS	O: H_3PO_4	DC: 100-200 A/m^2	0.5 M $CoSO_4$ 7.7 mM $H_2[PtCl_6]$ 50 mL/L CH_3COOH	pH = 3.5 (CH_3CO ONa), 313 K	Detailed structural studies of AAO and nanowires	[103]
Co-Zn	LO	-	AC: 15 V, 200 Hz	30 g/L $FeSO_4 \cdot 7H_2O$ 5 g/L $ZnSO_4 \cdot 7H_2O$, 10 g/L H3BO4	pH = 3 (H_2SO_4) 5 min	Magnetic Properties of NWs were studied	[104]
Cu	LS	BLT: H_2SO_4	AC: 10 V, 200 Hz	0.50 M $CuSO_4$ 0.285 M H_3BO_3	10-15 min	Multigram synthesis of the Cu NWs	[105]
Cu	LO/LS	RO: $SnCl_4$, H_3PO_4	DC: 0.3 V	0.2 M $CuSO_4 \cdot 5H_2O$ 0.1 M H_3BO_3	RT, 20-30 min	Y-branched Cu NW were formed	[67]
Cu	C	C: Whatman (Anopore)	DC: 50 mA/cm2	0.5 M $CuSO_4 \cdot 5H_2O$	pH = 1, RT	Kinetics of growth of Cu NW was studied	[106]
Cu	LO	-	DC: 0.4 V	0.2 M $CuSO_4 \cdot 5H_2O$ 0.1 M H_3BO_3	pH = 3.0 (H_2SO_4) 25 ^oC	Cu NW were grown on NiTi shape memory alloy thin film	[107]
Cu	LS, LO	-	AC and Pulse	0.5 M $CuSO_4$ 0.57 M H_3BO_3 or 1.0 M $CuSO_4$ 0.57 M H_3BO_3	-	Wave shape and pulse polarity influence on AAO pore filling was investigated	[108]
Cu	LS, LO, LP	RO: $HgCl_2$, H_3PO_4	DC: 2 mA/cm2	0.5 M $CuSO_4$ 0.5 M H_2SO_4	RT, 30 min	Large Cu foils (ca. 2 cm^2) were covered by Cu NW arrays	[58]
Fe	L	RO: $CuCl_2$, H_3PO_4	DC: 0.9-1.4 V	0.1, 0.5 or 1.0 M $FeSO_4 \cdot 7H_2O$ 0.525 M Na_2SO_4. 0.4 M H_3BO_3	pH = 3.0 (H_2SO_4 or NaOH), 5 - 10 min	Influence of the electrodeposition conditions on the morphology and resulting magnetic properties was investigated	[63]

Table 12.1, *(continued, part 6 of 10).*

NW metal	Type of AAO	Membrane preparation	Type of applied current	Deposition bath	Deposition conditions	Remarks / Investigated properties	Reference
Fe	LS, LO	-	AC: 0.25 A/dm2 50 Hz	0.1M FeSO4 0.025M MgSO4 0.1M citric acid additionally 0.5g/L 57Fe in form of sulfate salt	17 oC, 20-40 min	Detailed structural analysis of the Fe NWs was done	[109]
Fe	LO	BLT: acetone: $HClO_4$ 1:1 (vol.) 110 V, 4 ^oC, 5 min, subsequent etching in 5% H_3PO_4	DC: 2.0 V	120 g/L $FeSO_4 \cdot 7H_2O$, "a small amount of" $FeCl_3$ 45 g/L H_3BO_3 1 g/L ascorbic acid	pH = 2.0, 25 ^oC, 10 min	Magnetic Properties of NWs were studied	[76]
Fe-Pd	LS	-	AC: 25 V, 50 Hz	0.02 M $Pd(NH_3)_2Cl_2$ various concentration of $FeSO_4 \cdot 7H_2O$ and $C_7H_6O_6 \cdot 2H_2O$ 0.3 M $(NH_4)_2SO_4$	RT	Magnetic Properties of NWs were studied	[110]
Fe-Pt	LS	O: H3PO4	DC: 200-300 A/m^2	0.5 M $FeSO_4$ 7.7 mM $H_2[PtCl_6]$ 50 mL/L CH_3COOH	pH = 2.9 (CH_3CO ONa), 298 K	Detailed structural studies of AAO and nanowires	[103]
Ni	LO	-	DC: 10 mA/cm^2	Ni-sulfamate commercial plating bath (Technic, Inc.)	-	Voltage-current characteristics of single Ni NW were measured	[111]
Ni	L	-	DC: 3-4 mA/cm^2	$NiCl_2.6H_2O$ $Ni(H_2NSO_3)$. $4H_2O$ boric acid ascorbic acid	pH = 3.5 20 ^oC 5-15 min	Magnetic properties of obtained NW were studied	[112]
Ni	LO	RO: 10% Br_2 in CH_3OH (RT), H_3PO_4 + CrO_3	DC: -0.85 V	20 g/l H_3BO_3 20 g/l $NiCl_2 \cdot 6H_2O$ 160 g/l $NiSO_4 \cdot 7H_2O$	RT	Magnetic properties of obtained NW were studied	[70]
Ni	LS	-	Pulse: 2 mA/cm^2 2 h 30 ms each pulse	350 g/l NiSO4·7H2O 50 g/L NiCl4·7H2O 40 g/L H3BO3	pH = 4.5-5.5 45 – 55 ^oC	Structural studies (XRD, HR TEM) of the Ni NW were done	[113]

Table 12.1, *(continued, part 7 of 10).*

NW metal	Type of AAO	Membrane preparation	Type of applied current	Deposition bath	Deposition conditions	Remarks / Investigated properties	Reference
Ni	LO	RO: $SnCl_4$ + H_3PO_4	DC: 1.5 V	0.2 M $NiSO_4 \cdot 6H_2O$ 0.1 M H_3BO_3	pH = 2.0 (H_2SO_4)	Microscopic and magnetic studies of the Ni NW were carried out	[68]
Ni	LS, LO, LP	-	DC: 1.0-1.5 V	0.38 M $NiSO_4$ 0.13 M $NiCl_2$ 0.65 M H_3BO_4 60 ppm $CH_3(CH_2)_{11}OSO_3Na$	pH = 5.2 303 K 2-10 min	Ni NW were formed on the ITO glass	[114]
Ni	LO	O: H_3PO_4, BLT: 290 and 135 mA/cm^2	Pulse: -70 mA/cm^2 8 ms	300 g/L $NiSO_4 \cdot 6H_2O$ 45 g/L $NiCl_2 \cdot 6H_2O$ 45 g/L H_3BO_3	pH = 4.5 35 ^oC	The Ni NW were obtained in AAO with high filling factor	[115]
Ni	LO	RO: $SnCl_4$, H_3PO_4	DC: 2.1 V	80g/L $NiSO_4 \cdot 6H_2O$ 20g/L H_3BO_3 1.5g/L $C_6H_8O_7 \cdot H_2O$	RT	Y-branched Ni NW were formed	[69]
Ni	LP	BLT: H_3PO_4 / $(COOH)_2$ from 160 to 1.5 V	DC: 3.5 V	-	-	Cold field electron emission from Ni NW was researched	[116]
Ni	LS	RO: 0.1M $CuCl_2 \cdot 2H_2O$ in 6.1M HCl + 0.52 M H_3PO_4	DC: 3–5 mA/cm2	0.35 mol dm−3 $NiSO_4$	30 min	Diameter modulated Ni NW were formed	[61]
Ni		BLT: 8, 15, 20 V	AC: 3-6 V, 8-12 V, 12-16 V in respect to the BLT voltages 10-750 Hz	0.05 M $NiCl_2$ in DMSO	130 ± 0.5 °C	Ni NWs were deposited via electrochemical deposition from non-aqueous bath	[91]
Ni	LO	O: H_3PO_4	DC: -1.0 V	$NiSO_4.6H_2O$ (120 g/l), H_3BO_3 (45 g/l)	-	Magnetic properties of obtained NW were studied	[93]
Ni	LO	BLT: acetone: $HClO_4$ 1:1 (vol.) 110 V, 4 ^oC, 5 min, subsequent etching in 5% H_3PO_4	DC: 2.0 V	300 g/L $NiSO_4 \cdot 6H_2O$ + 45 g/L $NiCl_2 \cdot 6H_2O$ + 45 g/L H_3BO_3	pH = 4.0 25 oC, 15 min	Magnetic Properties of NWs were studied	[76]

Table 12.1, *(continued, part 8 of 10).*

NW metal	Type of AAO	Membrane preparation	Type of applied current	Deposition bath	Deposition conditions	Remarks / Investigated properties	Reference
Ni	LO	BLT: Various procedures were applied	Pulse: Cathodic, galvanostatic: 70 $mA \cdot cm^{-2}$, 8 ms Potentiostatic: 3 V, 2 ms Open circuit: 1 s	Watts type	-	Influence of the conditions on the BLT performance was studied in details; Y-branched Ni NWs were formed and structurally analyzed	[117]
Ni	LO	RO: 0.2 M $CuCl_2$ in 4.1 M HCl + 0.5 M H_3PO_4	Various electrochemical procedures, deriving from the systemic electrochemical studies of Ni electrodeposition were applied to form arrays of Ni NW				[65]
Ni	LO	BLT: from 40 to 8 V in $(COOH)_2$	Pulse	300 g/L $NiSO_4 \cdot 6H_2O$ 300 g/L $NiCl_2 \cdot 6H_2O$ 45 g/L H_3BO_3	40 ^oC	Magnetic properties of Ni NW with Au and Cu at the bottoms were investigated	[118]
Ni	LS, LO	BLT: 1 V for every 20 s; at 15 V the step was 15 min long O: H_3PO_4 after the BLT Cathodic polarization: 0.5 M KCl, 0 ^oC, -2.5 V, 5 min	Pulse: Negative: -17 V, 8 ms Positive: 3 V, 2 ms Open Circuit: 500 ms	300 g/L $NiSO_4 \cdot 6H_2O$ 45 g/L $NiCl_2 \cdot 6H_2O$ 45 g/L H_3BO_3	pH = 4.5 (H_3BO_3) 35 ^oC	The BLT process was studied in details; magnetic properties of Ni NW were investigated.	[119]
Ni	LO	RO: $HgCl_2$ + H_3PO_4	DC	200 g/L $NiCl_2 \cdot H_2O$ 120 g/L $NiSO_4 \cdot 7H_2O$ 50 g/l H_3BO_4	pH = 4 (NaOH) 25 ^oC	Magnetic properties of the Ni NW were examined	[59]
Ni	L	-	Pulse	-	-	Magnetic properties of the Ni NW were examined	[120]
Ni	LS, LO, LP	O: H_3PO_4	DC: 1.0-1.5 V	0.38 M $NiSO_4$ 0.13 M $NiCl_2$ 0.65 M H_3BO_4 60 ppm $CH_3(CH_2)_{11}OSO_3Na$	pH=5.2 (NaOH) 30 °C 2-10 min	Optical and magnetic properties of Ni NW deposited on ITO glass substrate were researched	[121]

Table 12.1, *(continued, part 9 of 10).*

NW metal	Type of AAO	Membrane preparation	Type of applied current	Deposition bath	Deposition conditions	Remarks / Investigated properties	Reference
Ni-Fe	LO	RO: $CuCl_2$ in HCl_2 + Reactive Ion Etching ($CF_2 + O_2$)	Pulse: -0.7 to -1.2 V	300 g/L $NiSO_4 \cdot 6H_2O$ 45 g/L $NiCl_2 \cdot 6H_2O$ 45 g/L H_3BO_3 6 g/L $FeSO_4 \cdot 6H_2O$	pH=2.8 25 °C	A systemic study of the influence of the deposition conditions on chemical composition of the NW on their structure and magnetic properties was done	[64]
Ni-Pt	LS	O: H_3PO_4	DC: 100-200 A/m^2	0.5 M $NiSO_4$ 7.7 mM $H_2[PtCl_6]$ 0.65 M H_3BO_3	pH = 4.0 ($CH_3CO ONa$), 298 K	Detailed structural studies of AAO and nanowires	[103]
Pd	LO	-	Pulse: -15 mA/cm^2	Commercial bath Palladure 150 and $Pd(NH_3)_4Cl_2$	-	Pd NWs dense arrays were formed on Ti coated silicon substrate	[122]
Pd	LO	RO: $CuSO_4$ in HCl + H_3PO_4	DC: 2 mA/cm^2	1 mg/L $Pd(NO_3)_2$ 0.5 M HNO_3	60 min	Pd NWs were formed in AAO templates made with the use of technical purity aluminum what allowed to cut costs of nanofabrication	[66]
Pd	LS, LO	RO: $HgCl_2 + H_3PO_4$	DC: -0.3 V	70 mM K_2PdCl_4 20 mM H_2SO_4 Pd	-	Structural studies of the Pd NWs (FE-SEM, XRD)	[123]
Pt	C	C: Whatman	DC	0.01 M $(Pt(NH_3)_2(NO_2)_2)$		Various experimental procedures were tested	[92]
Pt	LO	O: H_3PO_4 BLT: -10 V, 0.3 M $(COOH)_2$ ("till bubbles appeared")	DC: 10 mA/cm^2	A commercial Pt–DNS bath (Metakem, containing 5 g Pt/L)	pH = 2.5 60 °C	Electrochemical methanol decomposition on Pt NWs was performed	[124]
Pt	LS	O: H_3PO_4	DC: 0 V	5 mM H_2PtCl_6 1.2 mM HCl	RT	Electro-oxidation of methanol on Pt NWs was investigated, including stability of the NWs for many cycles of the electrochemical reactions	[125]

Table 12.1, *(continued, part 10 of 10).*

NW metal	Type of AAO	Membrane preparation	Type of applied current	Deposition bath	Deposition conditions	Remarks / Investigated properties	Reference
Sn	LO	-	AC: 80 V, 200 Hz	0.05 M $SnCl_2 \cdot 2H_2O$	pH = 1 (HCl)	The Sn NW were heated to form Sn/SnO_2 core-shell NWs	[126]
Sn	LO	RO: $HgCl_2$ + H_3PO_4	DC: 2 mA/cm^2	7 g dm^{-3} $SnCl_2$ + 25 g dm^{-3} sodium citrate	30 min, RT	AAO templates were formed on technical purity Al, instead of high purity Al, what allowed to cut costs significantly	[53]
Sn	LO	RO: $HgCl_2$ + H_3PO_4	DC: 0.5mA/cm^{-2}	7 g dm^{-3} $SnCl_2$ + 25 g dm^{-3} sodium citrate	30 min	AAO templates were formed at 20 ^{o}C and filled with Sn NW	[55]
Zn	LO	-	-	-	-	Lattice parameter changes of Zn NW in comparison to the bulk Zn were investigated	[127]

Template-assisted electrochemical fabrication of semiconducting and polymeric nanowires

Since nanowires are quasi-1D structures, manufacturing them is also attractive for different types of chemical compounds, especially semiconducing materials. According to the quantum-limited dimensions in two directions, one can expect significant modification of the material properties to result from the spatial confinement effect of the electrons. The concept of the electrochemical deposition of the nanowires made of organic and inorganic compounds - as well as metalloids - is analogous to the one presented for metallic nanowires (Fig. 12.8). After the deposition process the template is being removed, and hexagonal arrays of the nanowires are formed.

With the use of AAO-assisted electrochemical deposition, nanowires made of Ag_2S [128], $Bi_2Te_{2.7}Se_{0.3}$ [129], CdS [77, 130-133], CdTe [134], CoFeB [135], Cu_2O [136], CuS [128], CoSb [137], In_2S_3 [138], InSb [139], Se [140], SnO_2 [141], PbS [142], ZnO [143-144] were formed (Table 12.2). Mostly, optical properties of the nanowires made of CdS [130-132], Cu_2O [136], In_2S_3 [138], Se [140], and PbS [142] were investigated. Nanowires made of CdS [130-131, 133] and $Bi_2Te_{2.7}Se_{0.3}$ [129] allows the harvesting of energy more efficiently than traditionally shaped and sized materials, due to the improvements in photovoltaics (CdS) and thermoelectrics ($Bi_2Te_{2.7}Se_{0.3}$) properties. Arrays of inorganic nanowires, such

as those made of CoSb [137], may serve as electrodes with high surface area in lithium-ion batteries. Therefore, with the use of inorganic nanowires improvements in renewable energy harvesting and storage applications can be achieved.
Nanowires made of polypyrrole, obtained via electrochemical polimerization in the pores of AAO, have also attracted attention, thanks to their functional properties (Table 12.3) [145-146]. Their physical properties such as field emission are researched [145]. The high surface area provided by the formation of the nanowires makes them promising as components of electrochemical sensors [146]. See Section 'Electrochemical sensors based on nanowires' for a detailed review of these applications.

Template-assisted electrochemical fabrication of metallic nanotubes

Manufacturing of metallic nanotubes with electrochemical methods from an AAO template is challenging because the AAO is an insulator. In most cases, to provide metal deposition into the AAO pores in the form of hollow nanotubes, conductivity on the pores interior has to be ensured. Two major approaches have been developed. The first method is based on the surface chemistry of AAO [147-148]. According to Lee et al. [147], reduction of Ag^{2+} with Sn^{2+} allows to form compact, conductive film on the pore walls. During electrocrystallization the desired metal reduces on both pore bottoms and pore walls. Nevertheless, this method employs also chemistry of colloids to ensure adequate quality of the silver deposit. Moreover, in the above experiment multisegment Au-Ni nanotubes were formed [147], what additionally confirms the utility of the presented AAO surface modification method. Bao et al. reported silanization of the inner surface of the pores as an effective method to ensure electrical conductivity [148], allowing to successfully form metallic nanotubes. Alternatively to these sophisticated chemical methods, researchers often use the common and easy process of Au sputtering [149-154].

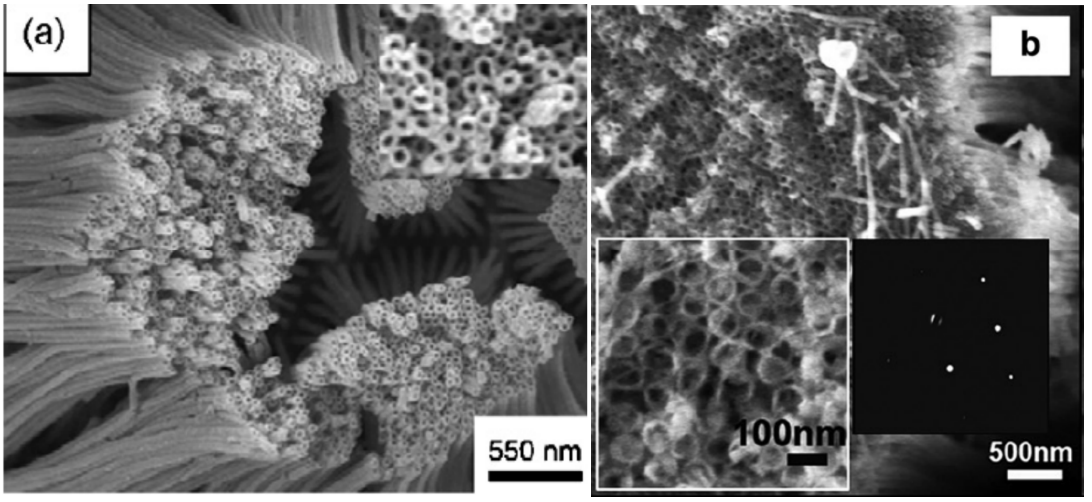

FIGURE 12.9
FE-SEM micrographs of nanotubes made of Ni (a) [154], Fe (b) [152]. Reprint with permission from Elsevier

TABLE 12.2
Gathers nanowires made of semiconductors and inorganic compounds with their fabrication conditions. Type of AAO: L – lab made (LS – sulfuric acid, LO – oxalic acid, LP – phosphoric acid), C – commercial. Type of membrane preparation: RO – chemical Al removal + pore opening (specified chemicals), O – chemical pore opening, BLT – electrochemical barrier layer thinning (specified conditions). Type of applied current: DC - DC electrodeposition, AC – AC electrodeposition, CV – Cyclic Voltammetry, Pulse – Pulse electrodeposition; RT – room temperature. *(Part 1 of 3, to be continued).*

NW material	Type of AAO	Membrane preparation	Type of applied current	Deposition bath	Deposition conditions	Remarks / Investigated properties	Reference
Ag_2S	-	-	DC: 0.3–0.8 mA/cm^2 Next: DC: 0.2-0.5 mA/cm^2	$AgNO_3$ – based solution Next: 0.01 M Na_2S	pH = 12.0 (sulfurization)	Ag_2S NWs were formed	[128]
$Bi_2Te_{2.7}Se_{0.3}$	C	C: Whatman	DC: -0.638 V	2.5 mM $Bi(NO_3)_3 \cdot 5H_2O$ 2 mM TeO_2 0.3 mM SeO_2 0.1M HNO_3	-	Single crystalline NWs were formed; prospective thermoelectric material	[129]
CdS	LP	-	DC: 0.8 V	0.2 M $CdSO_4$ 0.01M $Na_2S_2O_3$	pH = 2-3 (HCl)	Luminescent and photovoltaic properties of CdS NWs were researched	[130]
CdS	LO	O: H_3PO_4	DC: 10 V	0.055M $CdCl_2$ 0.19M elemental sulfur	120 ^oC 8-30 min	Luminescent and photovoltaic properties of CdS NWs were researched	[131]
CdS	LS	-	DC: 1 mA/cm^2	0.1 M $CdSO_4$ 0.1 M $Na_2S_2O_3$	RT 5 min	Optical properties were investigated	[132]
CdS	LS, LO, LP	BLT: to 5 V for 5 min O: H_3PO_4	AC: 30-50 V 60-500 Hz	0.055 M $CdCl_2$ 0.19 M elemental sulfur	100-160 ^oC 5-60 min	Electrochemical deposition from DMSO solution was conducted; structural analysis of the NWs was done	[77]
CdS	LO	-	DC: 7.5 mA/cm^2	0.055 M $CdCl_2$ 0.19M elemental sulfur	120 ^oC	Electrochemical deposition from DMSO solution was conducted; Photovoltaic properties were researched; Power conversion efficiency up to 17% was achieved	[133]

Table 12.2*, (continued, part 2 of 3).*

NW material	Type of AAO	Membrane preparation	Type of applied current	Deposition bath	Deposition conditions	Remarks / Investigated properties	Reference
CdTe	LO	-	DC: -0.58 V	1M $CdSO_4$ $3 \cdot 10^{-4}$ M TeO_2	pH = 2 (H_2SO_4) 8 h	Structural research	[134]
CoFeB	-	-	AC	-	-	Magnetic properties of NWs were researched	[135]
Cu_2O	C	C: Whatman	DC: 0.1-0.5 mA/cm^2	45 g of $CuSO_4$ dissolved in 75 mL of 88% lactic acid	pH = 6.0-12.0 (NaOH) 65 ^oC	Photoluminescence of Cu_2O NWs was investigated	[136]
CuS	-	-	DC: 0.3–0.8 mA/cm^2 Next: DC: 0.2-0.5 mA/cm^2	$CuSO_4$ – based solution Next: 0.01 M Na_2S	pH = 12.0 (sulfurization)	CuS NWs were formed and structurally characterized	[128]
CoSb	-	-	Pulse: 2.6 V	0.01 M $KSbOC_4H_4O_6 \cdot 2H_2O$ 0.2 M $CoCl_2 \cdot 6H_2O$ 0.18 M H_3BO_3	pH = 3.5 300 K	CoSb NWs were fabricated and investigated as a prospective materials for Li-ion batteries	[137]
In_2S_3	LO	RO: $HgCl_2 + H_3PO_4$	DC	$In(SO_4)_3$, H_3BO_3	-	In NW were sulfurized; β-In_2S_3 were obtained; structural and optical examinations	[138]
InSb	LO	RO: $HgCl_2 + H_3PO_4$	DC: -1.5 V, 10-220 mA/cm^2 Pulse: -2.1 V (0.5 s), 0 V (1 s)	0.15 M citric acid 0.06 M sodium citrate indium and antimony cations at a ratio of 4:1. 0.2 M citric acid, 0.15 M sodium citrate 0.06 M In^{3+} 0.045 M Sb^{3+}	40 min 120 min	DC and Pulse electrodeposition were performed; the influence of the applied electrochemical method on the composition of the NW was investigated	[139]

Table 12.2, *(continued, part 3 of 3)*

NW material	Type of AAO	Membrane preparation	Type of applied current	Deposition bath	Deposition conditions	Remarks / Investigated properties	Reference
Se	LO	RO: $HgCl_2$ + H_3PO_4	DC: 1.0 V (0.2 A/dm^3)	50 g/L SeO_2 20 g/L H_3BO_3	pH = 2.0 30 ^oC	Structural and optical studies	[140]
SnO_2	LO	-	AC: 80 V, 200 Hz	0.05 M $SnCl_2 \cdot 2H_2O$	pH = 1 (HCl)	Sn NWs were oxidized to form Sn / SnO_2 core / shell NWs	[141]
PbS	LS	RO: $HgCl_2$ + H_3PO_4	AC: 12 V (60 Hz)	$PbCl_2$ Elemental sulfur in DMSO	-	Optical studies	[142]
ZnO	LO	RO: $HgCl_2$ + H_3PO_4	DC: -1.5 V	0.01 M $Zn(NO_3)_2$	pH = 3.5 23 ^oC (RT) 5400 s	Cathodically induced sol-gel deposition of ZnO in the form of NWs was done	[143]
ZnO	LO	RO: $CuCl_2$ in HCl + H_3PO_4	DC: -1.1 V	0.05 M $ZnCl_2$ in HCl	85 ^oC	ZnO NW were formed via electrodeposition from non-aqueous solution	[144]

TABLE 12.3
Gathers nanowires made of organic compounds, including polymers, with their fabrication conditions. Type of AAO: L – lab made (LS – sulfuric acid, LO – oxalic acid, LP – phosphoric acid), C – commercial. Type of membrane preparation: RO – chemical Al removal + pore opening (specified chemicals), O – chemical pore opening, BLT – electrochemical barrier layer thinning (specified conditions). Type of applied current: DC - DC electrodeposition, AC – AC electrodeposition, CV – Cyclic Voltammetry, Pulse – Pulse electrodeposition; RT – room temperature

NW material	Type of AAO	Membrane preparation	Type of applied current	Deposition bath	Deposition conditions	Remarks / Investigated properties	Reference
Polypyrrole	C	C: Whatman	DC: 0.8 V	75% isopropyl alcohol 20% boron trifluoride diethyl etherate 5% poly(ethylene glycol) 0.1 mol/L Pyrrole.	-	Field emission of the PPy NWs was researched	[145]
Polypyrrole	LO	RO: $HgCl_2$ + H_3PO_4	DC: 1.5 V (PPy) 0.8 V (PPy-HQS)	0.05 M pyrrole 0.05 M potassium hydroquinone monosulfonate one of the following: 0.1 M $NaClO_4$ 0.1 M $LiClO_4$ 0.1 M citric acid	100 s	The hydroquinone monosulfonate-doped polypyrrole NWs were obtained and applied as a pH sensor	[146]

Using the AAO template-assisted electrodeposition procedure, metallic nanotubes made of Au [149], Au-Ni [147], Co [92, 148, 150-151], Co-Pt [92], Fe [150, 152], Ni [150, 153-154] and Pt [92] were formed. Fabrication of these nanotubes was motivated mostly by the research on their magnetic [147, 151, 154] and catalytic properties [153] (Table 12.4).

Electrochemical sensors based on nanowires

The high surface area provided by conductive materials such as metals or conducting polymers deposited into the AAO nanopores, makes the resulting nanowire arrays attractive as electrodes. These materials play an important role in the energy storage as the active materials in lithium-ion batteries [82, 137]. However, the high surface area is also attractive in the field of electrochemical sensors, based on either voltammetry or impedance spectroscopy.

TABLE 12.4
Gathers metallic nanotubes with their fabrication conditions. Type of AAO: L – lab made (LS – sulfuric acid, LO – oxalic acid, LP – phosphoric acid), C – commercial. Type of membrane preparation: RO – chemical Al removal + pore opening (specified chemicals), O – chemical pore opening, BLT – electrochemical barrier layer thinning (specified conditions). Type of applied current: DC - DC electrodeposition, AC – AC electrodeposition, CV – Cyclic Voltammetry, Pulse – Pulse electrodeposition; RT – room temperature. *(Part 1 of 2, to be continued).*

NT material	Type of AAO	Membrane preparation	Formation of conductive layer	Type of applied current	Deposition bath	Deposition conditions	Remarks / Investigated properties	Reference
Au	LP	BLT + O (H_3PO_4)	Au sputtering	DC: 1.5 mA/cm^2	Commercial plating solution Auruna 5000	50 s 17 °C	Au NTs were formed	[149]
Au -Ni	LP	BLT	Surface redox reaction: $Ag^+ + Sn^{2+} \rightarrow Ag + Sn^{4+}$	DC: Au: 2.2-2.5 mA/cm^2 Ni: 2.4 mA/cm^2	Au: commercial plating solution Auruna 5000 Ni: 0.0841 mol/L $NiCl_2{\cdot}6H_2O$ 1.59 mol/L $Ni(H_2NSO_3)_2{\cdot}4H_2O$ 0.33 mol/L H_3BO_3	pH = 3.4 (CH_3CONa)	Au-Ni-Au-Ni-Au multi-segment NT were formed and their magnetic properties were investigated	[147]
Co	C	C: Whatman	Silanization (methyl-c-diethylenetriaminopropyl-dimethoxysilane in anhydrous nonane) + Au evaporation	DC: 0.5 mA/cm^2	20 g/L $CoSO_4{\cdot}7H_2O$ 35 g/ L H_3BO_3	293 K	Structural and magnetic studies	[148]
Co	C	C: Whatman	Au sputtering	DC: 0.2 mA/mm^2	266 g/L $CoSO_4{\cdot}7H_2O$ 40 g/L H_3BO_3	RT	Structural and mechanistic research	[150]
Co	C	C: Whatman	Au sputtering	DC	1 M $CoSO_4$	pH = 3.0 (H_2SO_4), RT, 360 min	Various experimental procedures were tested	[92]
Co	LO, LP	-	-	DC	1M $CoSO_4{\cdot}7H_2O$ 40 g/L H_3BO_3	-	Magnetic studies of Co nanorings (short tubes)	[151]

Table 12.4*, (continued, part 2 of 2).*

NT material	Type of AAO	Membrane preparation	Formation of conductive layer	Type of applied current	Deposition bath	Deposition conditions	Remarks / Investigated properties	Reference
Co -Pt	C	C: Whatman	Au sputtering	DC	0.1 M Cobalt sulphamate 0.01 M $(Pt(NH_3)_2(NO_2)_2)$, 0.1 M ammonium citrate 0.1 M glycine	pH = 8.0 (NaOH)	Various experimental procedures were tested	[92]
Fe	C	C: Whatman	Au sputtering	DC: 0.2 mA/mm^2	140 g/L $FeSO_4 \cdot 7H_2O$ 50 g/L H_3BO_3 1 g/L ascorbic acid	RT	Structural and mechanistic research	[150]
Fe	LP	-	Au sputtering	DC: 1.35 V	120 g/L $FeSO_4 \cdot 7H_2O$ 45 g/L H_3BO_3	50 ^oC	Structural studies of Fe NTs	[152]
Ni	C	C: Whatman	Au sputtering	DC: 0.2 mA/mm^2	270 g/L $NiSO_4 \cdot 6H_2O$ 40 g/L $NiCl_2 \cdot 6H_2O$ 40 g/L H_3BO_3	RT	Structural and mechanistic research	[150]
Ni	C	C: Whatman	Au sputtering	DC: 10 mA/cm^2	1.4 M $Ni(NH_2SO_3)_2 \cdot 4H_2O$ 0.5 M H_3BO_3	pH = 3.5	Ni NTs were examined as a cathode catalyst for hydrogen evolution reaction	[153]
Ni	LS, LO, LO	RO: $CuCl_2$ + H_3PO_4	Au sputtering	DC: 1.4 V	100 g/L $NiSO_4 \cdot 6H_2O$ 30g/L $NiCl_2 \cdot 6H_2O$ 40 g/L H_3BO_3	pH = 2.5 (H_2SO_4)	Structural and magnetic studies	[154]
Pt	C	C: Whatman	Au sputtering	DC	0.01 M $(Pt(NH_3)_2(NO_2)_2)$	pH = 6.5	Various experimental procedures were tested	[92]

One type of nanostructures most often used for detectors are poylpyrrole (Ppy) nanowire arrays for detection of glucose [155], ammonia [156-157] or pH [146]. For example, to form Ppy-based glucose biosensor, glucose oxidase was deposited inside the AAO pore walls prior to the electropolymerization of the pyrrole [155]. The arrays formed enable glucose to be detected even below 1 mM [155]. With the use of Ppy nanowires even ppm concentration of ammonia can be detected, while the Ppy nanowire arrays works as the working electrode in electrochemical sensor [156-157]. Moreover, Ppy hydroquinone-doped nanowires may serve as pH detectors in the range from 2 to 12 [146].

Metallic nanowires, formed with the use of manufacturing procedures described above, may serve as the working electrodes in low detection-limit sensors. For example gold nanowire-based electrochemical sensors may serve to detect Pb^{2+} cations [158] or chemical compounds that can reduce Cu^{2+} [159]. Silver nanowires arrays are reported to serve as a working electrode in sensors, and thanks to the high surface area of the working electrode the sensitivity reach levels of about 0.0266 μA $cm^{-2}\mu M^{-1}$ [146].
Therefore, application of electrochemical methods to perform template-assisted manufacturing allows to form highly-sensitive electrochemical sensors.

Conclusions

Electrochemical techniques based on at least partial self-organization process are an attractive alternative as compared to the traditional time consuming and expensive methods normally used for manufacturing of nanostructures. The geometry of the formed metallic, semiconductive or polymeric nanowires or nanotubes is controlled by the geometrical features of the templates, which depend in turn on the respective fabrication conditions. Significant achievements in the diverse fields of magnetism, optics, optoelectronics, sensing, renewable energy harvesting and storage, can be acknowledged to nanostructures obtained by electrochemical manufacturing techniques described in this chapter. These procedures represent a promising approach to be further developed in the future, with hopefully increasing and expanding applications also in the areas of biomedical devices and related diagnostics, for example in the field of drug-delivery and brain-machine neural interfaces.

References

1. Sulka G.D. Highly Ordered Anodic Porous Alumina Formation by Self-Organized Anodizing. In: Eftekhari A. (Ed.) Nanostructured Materials in Electrochemistry. Wiley-VCH Verlag; 2008. 1-116.
2. Sulka G.D., Stępniowski W.J. Structural features of self-organized nanopore arrays formed by anodization of aluminum in oxalic acid at relatively high temperatures. Electrochimica Acta 2009; 54 3683-3691.
3. Zaraska L., Kurowska E., Sulka G.D., Senyk I., Jaskuła M. The effect of anode surface area on nanoporous oxide formation during anodizing of low purity aluminum (AA1050 alloy). J. Solid State Electrochem. 2014; 18 361-368.
4. Parkuhitk V.P., Shersulsky V.I. Theoretical modelling of porous oxide growth on aluminium. J. Phys. D.: Appl. Phys. 1992; 25 1258-1263.
5. Pashchanka M., Schneider J.J. Origin of self-organisation in porous anodic alumina films derived from analogy with Rayleigh–Bénard convection cells. J. Mater. Chem. 2011; 21 18761-18767.
6. Diggle J.W., Downie T.C., Goulding C.W. Anodic oxide films on aluminum. Chem. Rev. 1969; 69 365-405.
7. Parkhutik V.P., Belov V.T., Chernyckh M.A. Study of aluminium anodization in sulphuric and chromic acid solutions-II. Oxide morphology and structure. Electrochimica Acta 1990; 35 961-966.

8. Parkhutik V.P., Albella J.M., Makushok Y.E., Montero I., Martinez-Duart J.M. Shershulskii V.I. Study of aluminium anodization in sulphuric and chromic acid solutions-I. Kinetics of growth and composition of oxides. Electrochimica Acta 1990; 35 955-960.
9. Wang J., Wang C.W., Li S.Y., Zhou F. The effect of oxalic and sulfuric ions on the photoluminescence of anodic aluminum oxide formed in a mixture of sulfuric and oxalic acid. Applied Physics A: Materials Science and Processing 2009; 94 939-942.
10. Stępniowski W.J., Norek M., Michalska-Domańska M., Bombalska A., Nowak-Stępniowska A., Kwaśny M., Bojar Z. Fabrication of anodic aluminum oxide with incorporated chromate ions. Applied Surface Science 2012; 259 324-330.
11. Stępniowski W.J., Norek M., Michalska-Domańska M., Nowak-Stępniowska A., Bombalska A., Włodarski M., Bojar Z. Incorporation of copper chelate ions into anodic alumina walls. Materials Letters 2013; 106 242-245.
12. Jaafar M., Navas D., Hernández-Vélez M., Baldonedo J.L., Vázquez M., Asenjo A. Nanoporous alumina membrane prepared by nanoindentation and anodic oxidation. Surf. Sci. 2009; 603 3155-3159.
13. Masuda H., Kanezawa K., Nishio K. Fabrication of Ideally Ordered Nanohole Arrays in Anodic Porous Alumina Based on Nanoindentation Using Scanning Probe Microscope. Chem. Lett. 2002; 12 1218-1219.
14. Liu C.Y., Datta A., Wang Y.L.. Ordered anodic alumina nanochannels on focused-ion-beam-prepatterned aluminum surfaces. Appl. Phys. Lett. 2001; 78 120-122.
15. Choi J., Schilling J., Nielsch K., Hillebrand R., Reiche M., Wehrspohn R.B., Gösele U. Large-area porous alumina photonic crystals via imprint method. Mat. Res. Soc. Symp. Proc. 2002; 722 L5.2.1.
16. Choi J., Nielsch K., Reiche M., Wehrspohn R.B., Gösele U. Fabrication of monodomain alumina pore arrays with an interpore distance smaller than the lattice constant of the imprint stamp. J. Vac. Sci. Technol. 2003; B 21 763-766.
17. Choi J., Wehrspohn R.B., Gösele U. Mechanism of guided self-organization producing quasi-monodomain porous alumina. Electrochim. Acta 2005; 50 2591–2595.
18. Asoh H., Nishio K., Nakao M., Tamamura T., Masuda H. Conditions for Fabrication of Ideally Ordered Anodic Porous Alumina Using Pretextured Al. J. Electrochem. Soc., 2001; 148 B152-B156.
19. Asoh H., Ono S., Hirose T., Nakao M., Masuda H. Growth of anodic porous alumina with square cells. Electrochim. Acta 2003; 48 3171-3174.
20. Masuda H., Yamada H., Satoh M., Asoh H., Nakao M., Tamamura T. Highly ordered nanochannel-array architecture in anodic alumina. Appl, Phys. Lett. 1997; 71 2770-2772.
21. Masuda H., Asoh H., Watanabe M., Nishio K., Nakao M., Tamamura T. Square and Triangular Nanohole Array Architectures in Anodic Alumina. Adv. Mater. 2001; 13 189-192.
22. Masuda H., Abe A., Nakao M., Yokoo A., Tamamura T., Nishio K. Ordered Mosaic Nanocomposites in Anodic Porous Alumina. Adv. Mater. 15; 2003 161-164.
23. Nakao M., Okui S., Tanaka H., Shibata Y., Yokoo A., Tamamura T., Masuda H. Fabrication of GaAs hole array as a 2D-photonic crystal and their application to photonic bandgap waveguide. Opt. Quantum Electron. 2002; 34 183-193.
24. Lee W., Ji W., Ross C.A., Gösele U., Nielsch K. Wafer-scale Ni imprint stamps for porous alumina membranes based on interference lithography. Small 2006; 2 978-982.
25. Matsui Y., Nishio K., Masuda H. Highly Ordered Anodic Porous Alumina by Imprinting Using Ni Molds Prepared from Ordered Array of Polystyrene Particles. Jap. J. Appl. Phys. 2005; 44 7726-7728.

26. Masuda H., Fukuda K. Ordered metal nanohole arrays made by a two-step replication of honeycomb structures of anodic alumina. Science 1995; 5216 1466-1468.
27. Stępniowski W.J., Zasada D., Bojar Z. First step of anodization influences the final nanopore arrangement in anodized alumina. Surf. Coat. Technol. 2011; 206 1416–1422.
28. Sulka G.D., Parkoła K.G. Anodising potential influence on well-ordered nanostructures formed by anodisation of aluminium in sulphuric acid. Thin Solid Films 2006; 515 338-345.
29. Sulka G.D., Parkoła K.G. Temperature influence on well-ordered nanopore structures grown by anodization of aluminium in sulphuric acid. Electrochim Acta 2007; 52: 1880-1888.
30. Zaraska L., Stępniowski W.J., Sulka G.D., Ciepiela E., Jaskuła M. Analysis of nanopore arrangement and structural features of anodic alumina layers formed by two-step anodizing in oxalic acid using the dedicated executable software. Appl. Phys. A 2014; 114: 571–577.
31. Zaraska L., Stępniowski W.J., Sulka G.D., Ciepiela E. The effect of anodizing temperature on structural features and hexagonal arrangement of nanopores in alumina synthesized by two-step anodizing in oxalic acid. Thin Solid Films 2013; 534 155-161.
32. Stępniowski W.J., Norek M., Michalska-Domańska M., Bojar Z. Ultra- small nanopores obtained by self-organized anodization of aluminum in oxalic acid at low voltages. Materials Letters 2013; 111 20-23.
33. Zaraska L., Sulka G.D., Jaskuła M. The effect of n-alcohols on porous anodic alumina formed by self-organized two-step anodizing of aluminum in phosphoric acid. Surf Coat Technol 2010; 204 1729-1737.
34. Nielsch K., Choi J., Schwirn K., Wehrspohn R.B., Gösele U. Self-ordering regimes of porous alumina: 10%-porosity rule. Nano Lett. 2002; 7 677-680.
35. Arurault L. Pilling-Bedworth ratio of thick anodic aluminium porous films prepared at high voltages in H_2SO_4 based electrolyte. Transactions of the Institute of Metal Finishing 2008; 86 51-54.
36. Stępniowski W.J., Bojar Z. Synthesis of anodic aluminum oxide (AAO) at relatively high temperatures. Study of the influence of anodization conditions on the alumina structural features. Surf. Coat. Technol. 2011; 206 265-272.
37. Yuan Z.H., Sun S.Q., Duan Y.Q., Wang D.J. Fabrication of Densely Packed AlN Nanowires by a Chemical Conversion of Al2O3 Nanowires Based on Porous Anodic Alumina Film. Nanoscale Res Lett. 2009; 4 1126–1129.
38. Montero-Moreno J.M., Sarret M., Műller C. Self-ordered porous alumina by two-step anodizing at constant current: Behaviour and evolution of the structure. Micropor. Mesopor. Mater. 2010; 136 68-74.
39. Chowdhury P., Raghuvaran M., Krishnan M., Barshilia H.C., Rajam K.S. Effect of process parameters on growth rate and diameter of nano-porous alumina templates. Bull. Mater. Sci. 2011; 34 423–427.
40. Huang G.S., Wu X.L., Yang L.W., Shao X.F., Siu G.G., Chu P.K. Dependence of blue-emitting property on nanopore geometrical structure in Al-based porous anodic alumina membranes. Appl. Phys A 2005; 81 1345–1349.
41. Choudhari K.S. Sudheendra P., Udayashankar N.K. Fabrication and high-temperature structural characterization study of porous anodic alumina membranes J. Porous. Mater. 2012; 19 1053-1062.
42. Ono S., Masuko N. Evaluation of pore diameter of anodic porous films formed on aluminum, Surf. Coat. Technol. 2003; 169-170 139-142.
43. Ono S., Saito M., Asoh H. Self-ordering of anodic porous alumina formed in organic acid electrolytes, Electrochim. Acta. 2005; 51 827-833.

44. Lee W., Ji R., Gösele U., Nielsch K. Fast fabrication of long-range ordered porous alumina membranes by hard anodization. Nature Mater. 2006; 5 741-747.
45. Sulka G.D., Brzózka A., Liu L. Fabrication of diameter-modulated and ultrathin porous nanowires in anodic aluminum oxide templates. Electrochim. Acta 2011; 56 4972-4979.
46. Santos A., Montero-Moreno J.M., Bachmann J., Nielsch K., Formentín P., Ferre-Borrull J., Pallares J., Marsal L.F. Understanding Pore Rearrangement during Mild to Hard Transition in Bilayered Porous Anodic Alumina Membranes. ACS Appl Mater Interfaces 2011; 3 1925–1932.
47. Zaraska L., Kurowska E., Sulka G.D., Jaskuła M. Porous alumina membranes with branched nanopores as templates for fabrication of Y-shaped nanowire arrays. J. Solid State. Electrochem. 2012 16 3611–3619.
48. Stępniowski W.J., Norek M., Michalska-Domańska M., Bombalska A., Nowak-Stępniowska A., Kwaśny M., Bojar Z. Fabrication of anodic aluminum oxide with incorporated chromate ions. Appl. Surf. Sci. 2012; 259 324-330.
49. Nishinaga O., Kikuchi T., Natsui S., Suzuki R.O. Rapid fabrication of self-ordered porous alumina with 10-/sub-10-nm-scale nanostructures by selenic acid anodizing. Scientific Reports 2013; 3 2748.
50. Kikuchi T., Yamamoto T., Natsui S., Suzuki R.O. Fabrication of anodic porous alumina by squaric acid anodizing. Electrochim. Acta 2014; 123 14-22.
51. Pashchanka M., Schneider J.J. Experimental validation of the novel theory explaining self-organization in porous anodic alumina films. Phys. Chem. Chem. Phys. 2013; 15 7070-7074.
52. Patra N., Salerno M., Losso R., Cingolani R. Use of unconventional organic acids as anodization electrolytes for fabrication of porous alumina, in: 2009 9th IEEE Conference on Nanotechnology, IEEE NANO 2009, Genoa, Italy, 26-30 July 2009 p. 567.
53. Zaraska L, Sulka GD, Jaskuła M. Porous anodic alumina membranes formed by anodization of AA1050 alloy as templates for fabrication of metallic nanowire arrays. Surf. Coat. Technol. 2010; 205: 2432–7.
54. Pang YT, Meng GW, Shan WJ, Zhang LD, Gao XY, Zhao AW, Mao YQ. Arrays of ordered Ag nanowires with different diameters in different areas embedded in one piece of anodic alumina membrane. Appl Phys A 2003; 77: 717-20.
55. Sulka GD, Brzózka A, Zaraska L, Jaskuła M. Through-hole membranes of nanoporous alumina formed by anodizing in oxalic acid and their applications in fabrication of nanowire arrays Electrochim Acta 2010; 55: 4368–76.
56. Zhang X, Li D, Bourgeois L, Wang H, Webley PA. Direct Electrodeposition of Porous Gold Nanowire Arrays for Biosensing Applications. Chem. Phys. Chem. 2009; 10: 436-41.
57. Zaraska L, Kurowska E, Sulka GD, Jaskuła M. Porous alumina membranes with branched nanopores as templates for fabrication of Y-shaped nanowire arrays. J. Solid State Electrochem. 2012; 16: 3611-9.
58. Zaraska L, Sulka GD, Jaskuła M. Fabrication of free-standing copper foils covered with highly-ordered copper nanowire arrays. Appl. Surf. Sci. 2012; 258: 7781-6.
59. Lin SW, Chang SC, Liu RS, Hu SF, Jan NT. Fabrication and magnetic properties of nickel nanowires. J. Magn. Magn. Mater. 2004; 282: 28-31.
60. Sun XY, Xu FQ, Li ZM, Zhang WH. Cyclic voltammetry for the fabrication of high dense silver nanowire arrays with the assistance of AAO template. Mat. Chem. Phys. 2005; 90: 69-72.
61. Sulka GD, Brzózka A, Liu L. Fabrication of diameter-modulated and ultrathin porous nanowires in anodic aluminum oxide templates. Electrochim Acta 2011; 56: 4972-9.
62. Vega V, Böhnert T, Martens S, Waleczek M, Montero-Moreno JM, Görlitz D, Prida VM, Nielsch K. Tuning the magnetic anisotropy of Co–Ni nanowires: comparison between single nanowires

and nanowire arrays in hard-anodic aluminum oxide membranes. Nanotechnology 2012; 23: 465709
63. Haehnel V, Fahler S, Schaaf P, Miglierini M, Mickel C, Schultz L, Schlörb H. Towards smooth and pure iron nanowires grown by electrodeposition in self-organized alumina membranes. Acta Mater 2010; 58: 2330–7.
64. Salem MS, Sergelius P, Zierold R, Montero Moreno JM, Görlitz D, Nielsch K. Magnetic characterization of nickel-rich NiFe nanowires grown by pulsed Electrodeposition. J. Mater. Chem. 2012; 22: 8549-57.
65. Proenca MP, Sousaa CT, Ventura J, Vazquez M, Araujo JP. Ni growth inside ordered arrays of alumina nanopores: Enhancing the deposition rate. Electrochim. Acta 2012; 72: 215-21.
66. Zaraska L, Kurowska E, Sulka GD, Senyk I, Jaskuła M. The effect of anode surface area on nanoporous oxide formation during anodizing of low purity aluminum (AA1050 alloy).J. Solid State Electrochem. 2014; 18: 361-368.
67. Gao T, Meng G, Zhang J, Sun S, Zhang L. Template synthesis of Y-junction metal nanowires. Appl Phys A 2002; 74: 403-6
68. Meng G, Cao A, Cheng JY, Vijayaraghavan A, Jung YJ, Shima M, Ajayan PM. Ordered Ni nanowire tip arrays sticking out of the anodic aluminum oxide template. J. Appl. Phys. 2005; 97: 064303.
69. Guo Q, Qin L, Zhao J,Hao Y, Yan Z, Mu F, Chen P. Structural analysis and angle dependent magnetic properties of Y-branched Ni nanowires. Physica E 2012; 44: 1988-91.
70. Napolskii KS, Eliseev AA, Yesin NV, Lukashin AV, Tretyakov YD, Grigoriev NA, Grigoriev SV, Eckerleb H. Ordered arrays of Ni magnetic nanowires: Synthesis and investigation. Physica E 2007; 37: 178–83.
71. Cui J., Wu Y., Wang Y., Zheng H., Xu G., Zhang X. A facile and efficient approach for pore-opening detection of anodic aluminum oxide membranes. Appl. Surf. Sci. 2012; 258: 5305-11.
72. Furneaux R.C., Rigby W.R., Davidson A.P. The formation of controlled-porosity membranes from anodically oxidized aluminium. Nature 1989; 337: 147-9.
73. Ghaffari M., Ramazani A., Almasi Kashi M. Improvement in the microstructure and magnetic properties in arrays of dc pulse electrodeposited Co nanowires induced by Cu pre-plating. J. Phys. D. Appl. Phys. 2013; 46: 295002.
74. Marquardt B., Eude L., Gowtham M., Cho G., Jeong H.J., Chatelet M., Cojocaru C.S., Kim B.S., Pribat D. Density control of electrodeposited Ni nanoparticles/nanowires inside porous anodic alumina templates by an exponential anodization voltage decrease. Nanotechnology 2008; 19: 405607.
75. Montero-Moreno J.M., Belenguer M., Sarret M., Müller C.M. Production of alumina templates suitable for electrodeposition of nanostructures using stepped techniques. Electrochim. Acta 2009; 54: 2529-35.
76. Qin J, Nogue J, Mikhaylova M, Roig A, Munoz JS, Muhammed M. Differences in the Magnetic Properties of Co, Fe, and Ni 250-300 nm Wide Nanowires Electrodeposited in Amorphous Anodized Alumina Templates. Chem. Mater. 2005; 17: 1829-34.
77. Routkevitch D, Bigioni T, Moskovits M, Xu JM. Electrochemical Fabrication of CdS Nanowire Arrays in Porous Anodic Aluminum Oxide Templates. J. Phys. Chem. 1996; 100: 14037-47.
78. Lee W, Alexe M, Nielsch K, Gösele U. Metal Membranes with Hierarchically Organized Nanotube Arrays. Chem. Mater. 2005; 17: 3325-7
79. Zhao X., Seo S.K., Lee U.J., Lee K.H. Controlled Electrochemical Dissolution of Anodic Aluminum Oxide for Preparation of Open-Through Pore Structures. J. Electrochem. Soc. 2007; 154 C553-7.

80. Vorobyova A.I., Outkina E.A., Komar O.M. Study of metal pillar nanostructure formation with thin porous alumina template. Thin Solid Films 2013; 548: 109-17.
81. Shaban M., Hamdy H., Shahin F., Park J., Ryu S.W. Uniform and Reproducible Barrier Layer Removal of Porous Anodic Alumina Membrane. J. Nanosci. Nanotechnol. 2010; 10: 3380-4.
82. Cheah SK, Perre E, Rooth M, Fondell M, Hårsta A, Nyholm L, Boman M, Gustafsson T, Lu J, Simon P, Edström K. Self-Supported Three-Dimensional Nanoelectrodes for Microbattery Applications. Nano Lett 2009; 9: 3230-3.
83. Choi J, Sauer G, Nielsch K, Wehrspohn RB, Gösele U. Hexagonally Arranged Monodisperse Silver Nanowires with Adjustable Diameter and High Aspect Ratio. Chem. Mater. 2003; 15: 776-9.
84. Zhang J, Kielbasa JE, Carroll DL. Controllable fabrication of porous alumina templates for nanostructures synthesis. Mat. Chem. Phys. 2012; 122: 295-300.
85. Chi GJ, Yao SW, Fan J, Zhang WG, Wang HZ. Antibacterial activity of anodized aluminum with deposited silver. Surf Coat Technol 2002; 157: 162–5.
86. Yasui A, Iwasaki M, Kawahara T, Tada H, Ito S. Color properties of gold–silver alternate nanowires electrochemically grown in the pores of aluminum anodic oxidation film. J. Colloid Interface Sci. 2006; 293: 443-8.
87. Lin SC, Chen SY,Chen YT, Cheng SY. Electrochemical fabrication and magnetic properties of highly ordered silver–nickel core-shell nanowires. J. Alloys Compds 2008; 449: 232–6.
88. Wu Z, Zhang Y, Du K. A simple and efficient combined AC–DC electrodeposition method for fabrication of highly ordered Au nanowires in AAO template. Appl. Surf. Sci. 2013; 265: 149-56.
89. Schröper F, Brüggemann D, Mourzina Y, Wolfrum B, Offenhäusser A, Mayer D. Analyzing the electroactive surface of gold nanopillars by electrochemical methods for electrode miniaturization. Electrochim. Acta 2008; 53: 6265–72.
90. Matsumoto F, Kamiyama M, Nishio K, Masuda H. Highly Ordered Nanopatterning of DNA with 40nm Diameter Using Anodic Porous Alumina Substrate. Jpn. J. Appl. Phys. 2005; 44: L355–8.
91. Yin AJ, Li J, Jian W, Bennet AJ, Xu JM. Fabrication of highly ordered metallic nanowire arrays by electrodeposition. Appl. Phys. Lett. 2001; 79: 1039-41.
92. Fu J, Cherevko S, Chung CH. Electroplating of metal nanotubes and nanowires in a high aspect-ratio nanotemplate. Electrochem. Commun. 2008; 10: 514-8.
93. Ohgai T, Hoffer X, Fabian A, Gravier L, Anserment JP. Electrochemical synthesis and magnetoresistance properties of Ni, Co and Co/Cu nanowires in a nanoporous anodic oxide layer on metallic aluminium. J. Mater. Chem. 2003; 13: 2530-4.
94. Strijkers GJ, Dalderop HJ, Broeksteeg MAA, Swagten HJM, de Jonge WJM. Structure and magnetization of arrays of electrodeposited Co wires in anodic alumina. J Appl Phys 1999; 86: 5141-5.
95. Cattaneo L, Franz S, Albertini F, Ranzieri P, Vicenzo A, Bestetti M, Cavallotti PL. Electrodeposition of hexagonal Co nanowires with large magnetocrystalline anisotropy. Electrochim. Acta 2012; 85: 57-65.
96. Yasui K, Morikawa T, Nishio K, Masuda H. Patterned Magnetic Recording Media Using Anodic Porous Alumina with Single Domain Hole Configurations of 63nm Hole Interval. Jpn. J. Appl. Phys. 2005; 44: L 469–L 71.
97. Foyet A, Hauser A, Schäfer W. Electrochemical deposition of the cobalt nanostructure by double template and pulse current methods. Mat. Sci. Eng. C 2007; 27: 100–4.
98. Vivas LG, Ivanov YP, Trabada DG, Proenca MP, Chubykalo-Fesenko O, Vazquez M. Magnetic properties of Co nanopillar arrays prepared from alumina templates. Nanotechnology 2013;

24: 105703.
99. Cho JU, Wu JH, Min JH, Lee JH, Liu HL, K YK. Effect of field deposition and pore size on Co/Cu barcode nanowires by electrodeposition. J. Magn. Magn. Mater. 2007; 310: 2420-2.
100. Fodor PS, Tsoi GM, Wenger LE. Zero magnetization states in electrodeposited Co0.45Fe0.55 nanowire arrays. J. Appl. Phys. 2003; 93: 7035-7.
101. Rosa WO, Vivas LG, Pirota KR, Asenjo A, Vázquez M. Influence of aspect ratio and anisotropy distribution in ordered CoNi Nanowire arrays. J. Magn. Magn. Mater. 2012; 324: 3679-82.
102. Atalay S, Kaya H, Atalay FE, Aydogmus E. Magnetoimpedance effects in a CoNiFe nanowire array. J. Alloys Compds. 2013; 561: 71-5.
103. Chu SZ, Inoue S, Wada K, Kurashima K. Fabrication of integrated arrays of ultrahigh density magnetic nanowires on glass by anodization and electrodeposition. Electrochim. Acta 2005; 51: 820–6.
104. Xu Y, Fu JL, Gao DQ, Xue DS. The fabrication and characteristic properties of amorphous Co1-xZnx alloy nanowires arrays. J Alloys Compds. 2010; 495: 450-2.
105. Gelves GA, Murakami ZTM, Krantz MJ, Haber JA. Multigram synthesis of copper nanowires using ac electrodeposition into porous aluminium oxide templates. J. Mater. Chem. 2006; 16: 3075–83.
106. Riveros G, Gomez H, Cortes A, Marotti RE, Dalchiele EA. Crystallographically-oriented single-crystalline copper nanowire arrays electrochemically grown into nanoporous anodic alumina templates. Appl Phys A 2005; 81: 17-24.
107. Bayat N, Sanjabi S, Barber ZH. Growth of copper nanowire arrays on NiTi shape memory alloy thin film. Surf. Coat. Technol. 2012; 206: 4075-8
108. Gerein NJ and Haber JA. Effect of ac Electrodeposition Conditions on the Growth of High Aspect Ratio Copper Nanowires in Porous Aluminum Oxide Templates. J Phys. Chem. B. 2005; 109: 17372-17385
109. Jagminas A, Mažeika K, Reklaitis J, Pakštas V, Baltrūnas D. Annealing effects on the transformations of Fe nanowires encapsulated in the alumina template pores. Mat. Chem. Phys. 2009; 115: 217-22.
110. Fei XL, Tang SL, Wang RL, Su HL, Du YW. Fabrication and magnetic properties of Fe–Pd nanowire arrays. Solid State Commun. 2007; 141: 25–8.
111. Choi DS, Rheem Y, Yoo B, Myung NV, Kim YK, I-V characteristics of a vertical single Ni nanowire by voltage-applied atomic force microscopy. Curr. Appl. Phys. 2010;10: 1037-40.
112. Oh SL, Kim YR, Malkinski L, Vovk A, Whittenburg SL, Kim EM, Jung JS. Magnetic properties of nickel nanostructures grown in AAO membrane. J. Magn. Magn. Mater. 2007; 310: e827–e9.
113. Han S, Chen HY, Chen CC, Yuan TN, Shih HC. Characterization of Ni nanowires after annealing. Mater. Lett. 2007; 61: 1105–8.
114. Chu SZ, Wada K, Inoue S, Todoroki S. Fabrication and characteristics of nanostructures on glass by Al anodization and electrodeposition. Electrochim. Acta 2003; 48: 3147-53.
115. Nielsch K, Müller F, Li AP, Gösele U. Uniform Nickel Deposition into Ordered Alumina Pores by Pulsed Electrodeposition. Adv. Mater. 2000; 12: 582-6.
116. Feizi E, Scott K, Baxendale M, Pal C, Ray AK, Wang W, Pang Y, Hodgson SNB. Synthesis and characterisation of nickel nanorods for cold cathode fluorescent lamps. Mat. Chem. Phys. 2012; 135: 832-6.
117. Montero-Moreno JM, Belenguer M, Sarret M, Műller CM. Production of alumina templates suitable for electrodeposition of nanostructures using stepped techniques. Electrochim. Acta 2009; 54: 2529-35.
118. Sousa, Leitao DC, Ventura J, Tavares PB, Araujo JP. A versatile synthesis method of dendrites-

free segmented nanowires with a precise size control. Nanoscale Res. Lett. 2012; 7: 168.
119. Winkler N, Leuthold J, Lei Y, Wilde G. Large-scale highly ordered arrays of freestanding magnetic nanowires. J. Mater. Chem. 2012; 22: 16627-16632.
120. Nielsch K, Wehrspohn RB, Barthel J, Kirschner J, Fischer SF, Kronmüller H, Schweinböck T, Weiss D, Gösele U. High density hexagonal nickel nanowire array. J. Magn. Magn. Mater. 2002; 249: 234-240.
121. Chu SZ, Wada K, Inoue S, Todoroki S. Fabrication and Characteristics of Ordered Ni Nanostructures on Glass by Anodization and Direct Current Electrodeposition. Chem. Mater. 2002; 14: 4595-602.
122. Kim K, Kim M, Cho SM. Pulsed electrodeposition of palladium nanowire arrays using AAO template. Mat. Chem. Phys. 2006; 96: 278-82
123. Kartopu G, Habouti S, Es-Souni M. Synthesis of palladium nanowire arrays with controlled diameter and length. Mat. Chem. Phys. 2008; 107: 226-30.
124. Holubowitch N, Nagle LC, Rohan JF. Porous alumina thin films on conductive substrates for templated 1-dimensional nanostructuring. Solid State Ionics 2012; 216: 110-3.
125. Zhao GY, Xu CL, Guo DJ, Li H, Li HL. Template preparation of Pt nanowire array electrode on Ti/Si substrate for methanol electro-oxidation. Appl. Surf. Sci. 2007; 253: 3242–6.
126. Kolmakov A, Zhang Y, Moskovits M. Topotactic Thermal Oxidation of Sn Nanowires: Intermediate Suboxides and Core-Shell Metastable Structures. Nano Lett. 2003; 8: 1125-9.
127. Wang Y, Zhao H, Hu Y, Ye C, Zhang L. Thermal expansion behavior of hexagonal Zn nanowires. J. Cryst. Growth 2007; 305: 8-11.
128. Liang C, Terabe K, Hasegawa T, Aono M. Template synthesis of M/M2S (M=Ag, Cu) hetero-nanowires by electrochemical technique. Solid State Ionics 2006; 177: 2527–31.
129. Li XL, Cai KF, Li H, Yu DH, Wang X, Wang HF. Alumina template-assisted electrodeposition of Bi2Te2:7Se0:3 nanowire arrays. Superlatt. Microstruct. 2010; 47: 710-3.
130. Kang Y and Kim D. Well-aligned CdS nanorod/conjugated polymer solar cells. Solar Energy Mater. Solar Cells 2006; 90: 166–74.
131. Aguilera A, Jayaraman V, Sanagapalli S, Suresh Singh R, Jayaraman V, Sampson K, Singh VP. Porous alumina templates and nanostructured CdS for thin film solar cell applications. Solar Energy Mater. Solar Cells 2006; 90: 713–26.
132. Gavrilov SA, Gusev VV, Dneprovski VS, Zhukov EA, Syrnikov AN, Muljarov EA. Optical properties of excitons in CdS semiconductor–insulator quantum wires. JETP Lett. 1999; 70: 216-21.
133. Liu P, Singh VP, Jarro CA, Rajaputra S. Cadmium sulfide nanowires for the window semiconductor layer in thin film CdS–CdTe solar cells. Nanotechnology 2011; 22: 145304
134. Zhao AW, Meng GW, Zhang LD, Gao T Sun SH, Pang YT. Electrochemical synthesis of ordered CdTe nanowire arrays. Appl. Phys. A 2003; 76: 537–9.
135. Sharif R, Zhang XQ, Shamaila S, Riaz S, Jiang LX, Han XF. Magnetic and magnetization properties of CoFeB nanowires. J. Magn. Magn. Mater. 2007; 310: e830–2.
136. Ko E, Choi J, Okamoto K, Tak Y, Lee J. Cu2O Nanowires in an Alumina Template: Electrochemical Conditions for the Synthesis and Photoluminescence Characteristics. Chem. Phys. Chem. 2006; 7: 1505–9.
137. Yang Y, Liu F, Li T, Chen Y, Wu Y,Kong M. Electrochemical performance of template synthesized CoSb nanowires array as an anode material for lithium ion batteries. Script. Mater. 2012; 66: 495-8.
138. Shi JB, Chen CJ, Lin YT, Hsu WC, Chen YC, Wu PF (2009) Anodic Aluminum Oxide Membrane-Assisted Fabrication of b-In2S3 Nanowires. Nanoscale Res Lett 4: 1059-63.

139. Hnida K, Mech J, Sulka GD. Template-assisted electrodeposition of indium–antimony nanowires – Comparison of electrochemical methods. Appl. Surf. Sci. 2013; 287: 252-6.
140. Zhang XY, Xu LH, Dai JY, Cai Y, Wang N. Synthesis and characterization of single crystalline selenium nanowire arrays. Mat. Res. Bull. 2006; 41: 1729–34.
141. Kolmakov A, Zhang Y, Moskovits M. Topotactic Thermal Oxidation of Sn Nanowires: Intermediate Suboxides and Core-Shell Metastable Structures. Nano Lett. 2003; 8: 1125-9.
142. Wu C, Shi JB, Chen CJ, Lin JY. Synthesis and optical properties of ordered 30 nm PbS nanowire arrays fabricated into sulfuric anodic alumina membrane. Mater. Lett. 2006; 60: 3618–21.
143. Öztürk S, Tasaltın N, Kılınç N, Yüzer H, Öztürk ZZ. Fabrication of ZnO nanowires at room temperature by cathodically induced sol–gel method. Appl. Phys. A 2010; 99: 73-8.
144. Gomez H, Riveros G, Ramirez D, Henriquez R, Schrebler R, Marotti R, Dalchiele E. Growth and characterization of ZnO nanowire arrays electrodeposited into anodic alumina templates in DMSO solution. Appl. Phys. A 2012; 16: 197-204.
145. Yan H, Zhang L, Shen J, Chen Z, Shi G, Zhang B. Synthesis, property and field-emission behaviour of amorphous polypyrrole nanowires. Nanotechnology 2006; 17: 3446–50.
146. Sulka GD, Hnida K, Brzózka A. pH sensors based on polypyrrole nanowire arrays. Electrochim. Acta 2013; 104: 536-41.
147. Lee W, Scholz R, Nielsch K, Gösele U. A Template-Based Electrochemical Method for the Synthesis of Multisegmented Metallic Nanotubes. Angew. Chem. Int. Ed. 2005; 44: 6050 –4.
148. Bao J, Xu Z, Hong J, Ma X, Lu Z. Fabrication of cobalt nanostructures with different shapes in alumina template. Scripta Mater 2004; 50: 19–23.
149. Lee W, Alexe M, Nielsch K, Gösele U. Metal Membranes with Hierarchically Organized Nanotube Arrays. Chem. Mater. 2005; 17: 3325-7
150. Cao H, Wang L, Qiu Y, Wu Q, Wang G, Zhang L, Liu X. Generation and Growth Mechanism of Metal (Fe, Co, Ni) Nanotube Arrays. Chem. Phys. Chem. 2006; 7: 1500–4.
151. Li YL, Tang SL, Xia WB, Chen LY, Wang Y, Tang T, Du YW. Large area Co nanoring arrays fabricated on silicon substrate by anodic aluminum oxide template-assisted electrodeposition. Appl Phys Lett 2012; 100: 183101.
152. Xu X, Huang J, Shao M, Wang P. Synthetic control of large-area, ordered Fe nanotubes and their nanotube-core/ alumina-sheath nanocables. Mat. Chem. Phys. 2012; 135: 6-9.
153. Yi Y, Lee JK, Lee HJ, Uhm S, Nam SC, Lee J. A single-step approach to create nanopottery structures for efficient water electrocatalysis. Electrochem. Commun. 2009; 11: 2121–4.
154. Wang XW, Yuan ZH, Fang BC. Template-based synthesis and magnetic properties of Ni nanotube arrays with different diameters. Mat. Chem. Phys. 2011; 125: 1–4.
155. Liu L, Jia N, Zhou Q, Yan M, Jiang Z. Electrochemically fabricated nanoelectrode ensembles for glucose biosensors. Mat. Sci. Eng. C. 2007; 27: 57-60.
156. Zhang L, Meng F, Chen Y, Liu J, Sun Y, Luo T, Li M, Liu J. A novel ammonia sensor based on high density, small diameter polypyrrole nanowire arrays. Sensors Actuators B 2009; 142: 204-9
157. Kim D, Yoo B. A novel electropolymerization method for Ppy nanowire-based NH_3 gas sensor with low contact resistance. 2011; 160: 1168-1173.
158. Zhang P, Xu G, Lv J, Cui J, Zheng Z, Wu Y. Fabrication of Au nanowire array for anodic stripping voltammetry determination of trace Pb^{2+} ions. J. Electroanal. Chem. 2012; 685: 91-9.
159. Samanman S, Thammakhet C, Kanatharana P, Buranachai C, Thavarungkul P. Novel template-assisted fabrication of porous gold nanowire arrays using a conductive-layer-free anodic alumina oxide membrane. Electrochim. Acta 2013; 102: 342-50.